

UNCLASSIFIED

AD 401 162

*Reproduced
by the*

DEFENSE DOCUMENTATION CENTER

FOR

SCIENTIFIC AND TECHNICAL INFORMATION

CAMERON STATION, ALEXANDRIA, VIRGINIA



UNCLASSIFIED

NOTICE: When government or other drawings, specifications or other data are used for any purpose other than in connection with a definitely related government procurement operation, the U. S. Government thereby incurs no responsibility, nor any obligation whatsoever; and the fact that the Government may have formulated, furnished, or in any way supplied the said drawings, specifications, or other data is not to be regarded by implication or otherwise as in any manner licensing the holder or any other person or corporation, or conveying any rights or permission to manufacture, use or sell any patented invention that may in any way be related thereto.

63-3-2

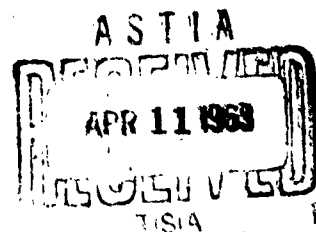
CATALOGED BY ASTIA
AS AD N8-1162

Office of Naval Research
Department of the Navy
Contract Nonr-220(24)

FLOW PAST A PARTIALLY CAVITATING CASCADE OF FLAT PLATE HYDROFOILS

by
R. B. Wade

401 162



Division of Engineering and Applied Science
CALIFORNIA INSTITUTE OF TECHNOLOGY
Pasadena, California

Report No. E-79-4

January 1963

Office of Naval Research
Department of the Navy
Contract Nonr-220(24)

**FLOW PAST A PARTIALLY CAVITATING CASCADE
OF FLAT PLATE HYDROFOILS**

by
R. B. Wade

**Division of Engineering & Applied Science
California Institute of Technology
Pasadena, California**

**Report No. E-79-4
January 1963**

**Approved by:
A. J. Acosta**

Notation

A, B, C	- constants
a	- modulus of f_2 , defined by equation (10)
c	- chord length
l	- length of cavity in ζ -plane
l_c	- length of cavity in z -plane
c_p	- pressure coefficient, equation (24)
C_L	- lift coefficient, equation (24a)
i	- $\sqrt{-1}$
K	- cavitation number, equation (1)
p	- pressure
t	- semi-circle plane
u	- velocity component in x -direction
v	- velocity component in y -direction
V	- modulus of velocity vector
w	- $u-iv$, complex velocity function
x, y	- coordinates of physical plane
z	- $x + iy$
α	- flow angle with respect to chord
β	- stagger angle
φ	- defined by equation (10)
Ψ_{1, n_1}	- defined by equation (18c)
Ψ_{2, n_2}	- defined by equation (19c)
ζ	- transformation plane
σ	- solidity $c/2\pi$
$()_1$	- denotes upstream conditions

- ()₂ - denotes downstream conditions
- ()_m - mean conditions
- ()' - perturbation quantities
- ($\bar{\quad}$) - complex conjugate quantity

Flow Past a Partially Cavitating Cascade of Flat Plate
Hydrofoils

1. Introduction

This report deals with the non-viscous, steady cavitating flow through a cascade of flat plate hydrofoils in two dimensions. The usual assumptions of incompressibility and irrotationality are made.

The motivation for this investigation is the present day interest in the high speed performance of lifting surfaces, such as in hydroplane boats and the behavior of propellers operating under cavitating conditions. A further area of interest is that of turbomachinery. The demand for smaller, more compact pumps and turbines, for any given performance, necessitates operation at higher speeds giving rise to cavitation conditions. Hence the problem at hand is not only of theoretical interest but is of practical importance.

The problem of the fully wetted cascade has been extensively treated, and can be found, for example, in a paper of Garrick^{(1)*} and in standard texts such as Robinson and Laurmann.⁽²⁾ The case of cavitating flow through a cascade of flat plates with infinitely long cavities was first treated by Betz and Petersohn using the classical hodograph method for free streamline flow attributed to Helmholtz.

* Numbers in parentheses refer to the references at the end of the text.

In dealing with cavitating cascade flows, hodograph methods became somewhat unwieldy, and this has led to the use of linearized methods for solving these problems. This method, first used by Tulin⁽³⁾ assumes that the cavity-body system forms a slender body and that a perturbation technique similar to that used in thin airfoil theory may be used. The use of the linearized method leads to the solution of a mixed boundary value problem. The use and application of this method is well illustrated by Parkin.⁽⁴⁾

The first published paper on linearized cavity flows through cascades, was by Cohen and Sutherland.⁽⁵⁾ They dealt with the problem of arbitrarily shaped hydrofoils with finite cavities, longer than the chord length. However, only results for the flat plate are presented in their paper. Subsequently, Acosta and Hollander⁽⁶⁾ dealt with the partial cavitation in a cascade of semi-infinite flat plates. This problem was recently treated using a hodograph method by Stripling and Acosta⁽⁷⁾ but no formal comparison was made between the two methods. Acosta⁽⁸⁾ also considered the case of the fully choked cascade of circular arc hydrofoils. A comparison was made with the results of the linearized method with those obtained by Betz and Petersohn; generally, a good agreement was found.

In the region where the cavity is less than the chord length, no results have been published to the knowledge of the author, for cascade flows. This case would provide a complete picture as to the behavior of these flows over the entire range from the fully wetted to the fully choked conditions.

II. Formulation of Problem

As illustrated in Figure 1, the cascade consists of an infinite array of flat plate hydrofoils having a stagger angle β . The chord length of each blade is c and the spacing of the hydrofoils in the direction of the stagger angle, is taken as 2π . Hence the solidity, $\sigma = c/2\pi$.

The flow approaches the cascade with velocity V_1 at an angle of attack α_1 . The flow is turned by the cascade so that far downstream the flow velocity V_2 is at an angle α_2 to the blade chord. The cavities spring from the leading edge and terminate on the upper surface of each hydrofoil. In keeping with the linearized theory the thickness of the cavity is assumed small compared with the blade spacing 2π . The boundary conditions on the free streamline of the cavity are then applied along the real axis, as are the conditions on the wetted surface of the hydrofoils.

The velocity field is now considered as a perturbation about the velocity V_1 . Although, in the neighborhood of the cascade a more natural characteristic velocity would be the vector mean velocity V_m , it is found more convenient to adopt V_1 , as V_m is undetermined a priori, since it depends on V_2 . In the calculation of the lift coefficient, however, the angle which the vector mean V_m makes with the blades, viz., α_m , is used so as to bring it in line with fully wetted cascade flows.

The governing parameter in cavity flows is the cavitation number K defined as

$$K = \frac{P_1 - P_c}{\frac{1}{2} \rho V_1^2} \quad (1)$$

where p_1 is the pressure at upstream infinity and p_c is the cavity pressure, which is a constant. Since the velocity is defined at any point as

$$V = (u, v) = (V_1 + u', v') \quad (2)$$

where u', v' are perturbation components assumed small, compared to V_1 we obtain by the use of Bernoulli's equation

$$K = \frac{V_c^2}{V_1^2} - 1$$

However, neglecting the squares of u', v' compared with V_1^2 , this becomes

$$K = \frac{2u_c'}{V_1}$$

$$\therefore u_c' = \frac{KV_1}{2}$$

On the wetted portion of the hydrofoils, $v=0$, i.e., there is no flow through the blades. A further condition that has to be met, is the closure condition which requires that the cavity-body system form a closed body. This condition can be expressed as

$$\oint_{\text{body}} dy = 0 \quad (3)$$

The above conditions, together with the requirement that the velocity be finite at the trailing edge, enable a unique solution for the problem to be determined.

Hence the conditions to be satisfied are:

- (a) $v = 0$ on the wetted portion of hydrofoil
- (b) $u_c = V_1(1 + \frac{K}{2})$ on the cavity
- (c) $V = V_1 e^{-i\alpha} l$ at upstream infinity

(d) the closure condition, viz.,

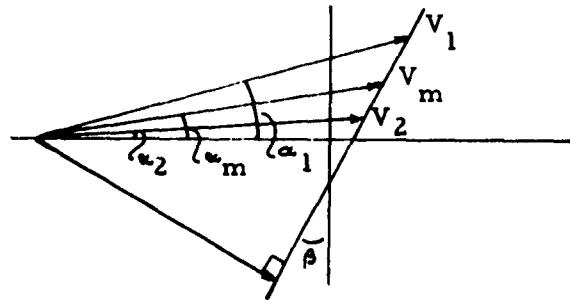
$$\oint_{\text{body}} dy = 0$$

(e) V is finite at the trailing edge.

These conditions are sufficient to determine the velocity function at every point including the downstream conditions where $V = V_2 e^{-i\alpha_2}$.

Before proceeding to solve the boundary value problem we derive the following simple relations from continuity considerations.

The velocity triangle is as follows



From this diagram we obtain

$$V_m \sin(\alpha_m + \beta) = \frac{1}{2} [V_1 \sin(\alpha_1 + \beta) + V_2 \sin(\alpha_2 + \beta)]$$

$$V_m \cos(\alpha_m + \beta) = V_1 \cos(\alpha_1 + \beta) = V_2 \cos(\alpha_2 + \beta) \quad (4)$$

from which we get

$$\tan(\alpha_m + \beta) = \frac{1}{2} [\tan(\alpha_1 + \beta) + \tan(\alpha_2 + \beta)] \quad (5)$$

III. Transformation Functions

Consider the transformation function

$$z = e^{-i\beta} \ln \frac{1 - \frac{\zeta}{\zeta_1}}{1 - \frac{\zeta}{\zeta_2}} + e^{i\beta} \ln \frac{1 - \frac{\bar{\zeta}}{\zeta_1}}{1 - \frac{\bar{\zeta}}{\zeta_2}} \quad (6)$$

This function maps the multiple-connected region in the z -plane onto the ζ -plane, as shown in Figures 2 and 3. The function has branch points at ζ_1 and ζ_2 in the ζ -plane, corresponding to the points $z = \mp \infty$, respectively. There is a branch cut between ζ_1 and ζ_2 . Hence when either point is encircled once, the argument of z changes by $\pm 2\pi e^{i(\pi/2 - \beta)}$. The sign depends on whether the branch point is encircled clockwise or counter-clockwise. Each Riemann sheet of the ζ -plane corresponds to the flow region over a different hydrofoil. Since the flow is periodic, however, the function is continuous across the cut.

The point $\zeta = 0$ corresponds to the point $z = 0$, as seen from equation (6). Further, when ζ is real, z must also be real, as it consists of the sum of complex conjugates. When ζ tends to infinity, we have

$$z \rightarrow e^{-i\beta} \ln \frac{\zeta_2}{\zeta_1} + e^{i\beta} \ln \frac{\bar{\zeta}_2}{\bar{\zeta}_1} \quad (7)$$

which is a real number.

Since $\zeta = 0$ is a singular point of the transformation, $dz/d\zeta = 0$ at $\zeta = 0$, i. e.,

$$e^{-i\beta} \left\{ \frac{\zeta_1 - \zeta_2}{\zeta_1 \zeta_2} \right\} + e^{i\beta} \left\{ \frac{\bar{\zeta}_1 - \bar{\zeta}_2}{\zeta_1 \zeta_2} \right\} = 0 \quad (8)$$

If we require that the trailing edge of the hydrofoil map into the point at infinity, then we must have $dz/d\zeta = 0$ at $\zeta = \infty$. However,

$$\frac{dz}{d\zeta} \text{ must } \rightarrow 0 \quad \text{as } \frac{1}{\zeta^3} \text{ at } \zeta \rightarrow \infty$$

This condition therefore gives

$$e^{-i\beta} (\zeta_1 - \zeta_2) + e^{i\beta} (\bar{\zeta}_1 - \bar{\zeta}_2) = 0 \quad (9)$$

Now let

$$\zeta_1 = r_1 e^{i\theta_1} = r_1 e^{i(\frac{\pi}{2} - \phi_1)}$$

$$\zeta_2 = r_2 e^{i\theta_2} = r_2 e^{i(\frac{\pi}{2} - \phi_2)}$$

so that

$$\theta_1 + \theta_2 = \pi - (\phi_1 - \phi_2)$$

$$\theta_1 - \theta_2 = -(\phi_1 + \phi_2)$$

With this notation, equations (8) and (9) reduce to

$$\frac{r_1}{r_2} = \frac{\cos(\frac{\pi}{2} - \beta + \phi_1)}{\cos(\frac{\pi}{2} - \beta - \phi_2)} \quad (8a)$$

$$\frac{r_1}{r_2} = \frac{\cos(\frac{\pi}{2} - \beta + \phi_2)}{\cos(\frac{\pi}{2} - \beta - \phi_1)} \quad (9a)$$

For these two equations to be compatible, we take $\varphi_1 = \varphi_2 = \varphi$; hence

$$\theta_1 + \theta_2 = \pi$$

$$\theta_1 - \theta_2 = -2\varphi$$

With these values, either equation (8a) or (9a) provides an equation for r_1/r_2 . Since the ratio of the moduli is the unknown, we are free to fix one of the moduli arbitrarily. Hence, we let $|\zeta_1| = r_1 = 1$ and $\zeta_2 = r_2 = a$, where $a > 1$. Then from either (8a) or (9a), we get

$$\tan \varphi = \frac{a-1}{a+1} \tan \beta \quad (10)$$

The transformation is now completely specified.

Since the trailing edge corresponds to the point at infinity, we get from equation (7)

$$c = 2 \cos \beta \ln a + 4\varphi \sin \beta \quad (11)$$

and hence the solidity σ is given by

$$\sigma = \frac{1}{\pi} \cos \beta \ln a + \frac{2\varphi}{\pi} \sin \beta \quad (12)$$

The point $z = l_c$ corresponding to the end of the cavity is mapped into a point on the positive real axis in the ζ -plane, $\zeta = l$. Thus, using the above notation together with equation (6), we get

$$l_c = 4 \cos \beta \ln \left[\frac{n_1}{n_2} \right] + 2 \sin \beta \gamma \quad (13)$$

where

$$n_1^4 = 1 + l^2 - 2l \sin \varphi$$

$$n_2^4 = 1 + l^2/a^2 + 2 \frac{l}{a} \sin \varphi$$

$$\gamma = \tan^{-1} \left[\frac{(a-1)l \cos \varphi + l^2 \sin 2\varphi}{a - (a-1)l \sin \varphi + l^2 \cos 2\varphi} \right]$$

We now transform the upper half ζ -plane into the half circle t -plane, Figure 4. To achieve this, we use the well known Joukowski transformation in the following form

$$\left(\zeta - \frac{l}{2}\right) = \frac{l}{4} \left(t + \frac{1}{t}\right) \quad (14)$$

In the t -plane the semi unit circle represents the constant pressure cavity surface and the real axis outside the unit circle represents the wetted portions of the hydrofoil. The leading edge is at the point $t = -1$, and the trailing edge at $t = \infty$.

The t -plane is used, since the velocity function for the given boundary conditions shown in Figure 4 can be written down by inspection.

IV. Solution of the Boundary Value Problem

The velocity function

$$w = u - iv = \frac{A}{t+1} + \frac{B}{t-1} + C \quad (15)$$

where A , B , and C are real constants, satisfies the boundary conditions for suitable values of A , B and C . This function corresponds to sources (or sinks) placed at the leading edge and at the end of the cavity. We now apply conditions (a) - (d) from page 4.

On the cavity, viz., $t = e^{i\theta}$, $(u_c, v_c) = (V_1 + u_c', v_c')$, therefore

$$u_c - iv_c = \frac{A}{2} \left[1 - i \tan \frac{\theta}{2} \right] - i \frac{B}{2} \left[\cot \frac{\theta}{2} - i \right] + C$$

hence

$$u_c = \frac{A-B}{2} + C$$

but

$$u_c = V_1 \left(1 + \frac{K}{2} \right)$$

thus

$$V_1 \left(1 + \frac{K}{2}\right) = \frac{A-B}{2} + C \quad (16)$$

Condition (a) is satisfied by equation (15) since when t is real, $v=0$. Further, condition (e) is obviously satisfied.

To apply the remaining conditions, it is more convenient to transform equation (15) back into the ζ -plane, by use of the transformation function (14). Inverting equation (14) we get

$$t = \frac{2}{\ell} \left[\left(\zeta - \frac{\ell}{2}\right) + \sqrt{\zeta(\zeta - \ell)} \right]$$

The positive root is taken because t tends to infinity as ζ tends to infinity. On substitution of this expression into equation (15), one obtains

$$w(\zeta) = \frac{A-B}{2} + C + \frac{B}{2} \sqrt{\frac{\zeta}{\zeta - \ell}} - \frac{A}{2} \sqrt{\frac{\zeta - \ell}{\zeta}} \quad (17)$$

Now

$$w(\zeta_1) = V_1 e^{-i\alpha_1}$$

Applying this condition to equation (17) and separating the resulting expression into real and imaginary parts, gives

$$V_1 \cos \alpha_1 = \left[\frac{A-B}{2} + C \right] + \frac{\cos \gamma_1}{2} \left[\frac{B}{n_1} - An_1 \right] \quad (18a)$$

$$V_1 \sin \alpha_1 = \frac{\sin \gamma_1}{2} \left[\frac{B}{n_1} + An_1 \right] \quad (18b)$$

where

$$\gamma_1 = \tan^{-1} \frac{\ell \cos \varphi}{1 - \ell \sin \varphi} \quad (18c)$$

$$n_1^4 = 1 + \ell^2 - 2\ell \sin \varphi$$

Now, applying the condition

$$w(\zeta_2) = V_2 e^{-i\alpha_2}$$

we get

$$V_2 \cos \alpha_2 = \left[\frac{A-B}{2} + C \right] + \frac{\cos \gamma_2}{2} \left[\frac{B}{n_2} - An_2 \right] \quad (19a)$$

$$V_2 \sin \alpha_2 = \frac{\sin \gamma_2}{2} \left[\frac{B}{n_2} + An_2 \right] \quad (19b)$$

where

$$\begin{aligned} \gamma_2 &= \tan^{-1} \frac{l \cos \varphi}{a + l \sin \varphi} \\ n_2^4 &= 1 + l^2/a^2 + 2l/a \sin \varphi \end{aligned} \quad (19c)$$

We finally have the closure condition, viz.,

$$\oint_{\text{body}} dy = 0$$

which reduces to

$$\text{Im pt} \frac{1}{V_1} \oint_{\text{body}} w(z) dz = 0$$

Since $w(z)$ is an analytic function in the flow region around the hydrofoils, we can deform the contour in the z -plane to the contour Γ shown in Figure 5. Then, symbolically we have

$$\oint_{\Gamma} w(z) dz = \oint_{\text{body}} + \int_H^A + \int_D^E + \lim_{\epsilon_1 \rightarrow 0} \int_{\epsilon_1} + \lim_{\epsilon_2 \rightarrow 0} \int_{\epsilon_2} w dz = 0$$

The contributions from the other parts of the contour cancel due to the periodicity of $w(z)$, while the contributions from the last two integrals in the above expression, are zero. Now

$$\left. \begin{array}{l} A \\ H \end{array} \right\} w(z)dz = 2\pi V_1 e^{-i(\alpha_1 + \beta)}$$

$$\left. \begin{array}{l} E \\ D \end{array} \right\} w(z)dz = -2\pi V_2 e^{-i(\alpha_2 + \beta)}$$

$$\therefore \text{Im pt } \frac{1}{V_1} \oint_{\text{body}} w(z)dz = \frac{2\pi}{V_1} \left[V_2 \cos(\alpha_2 + \beta) - V_1 \cos(\alpha_1 + \beta) \right] = 0$$

hence

$$V_1 \cos(\alpha_1 + \beta) = V_2 \cos(\alpha_2 + \beta) \quad (20)$$

This is the same result as already obtained by continuity considerations in equation (4). Finally we have the following equations to solve:

$$\frac{A-B}{2} + C = V_1 \left(1 + \frac{K}{2} \right)$$

$$V_1 \cos \alpha_1 = \frac{A-B}{2} + C + \frac{\cos \frac{\gamma_1}{2}}{2} \left[\frac{B}{n_1} - An_1 \right]$$

$$V_1 \sin \alpha_1 = \frac{\sin \frac{\gamma_1}{2}}{2} \left[\frac{B}{n_1} + An_1 \right]$$

$$V_2 \cos \alpha_2 = \frac{A-B}{2} + C + \frac{\cos \frac{\gamma_2}{2}}{2} \left[\frac{B}{n_2} - An_2 \right]$$

$$V_2 \sin \alpha_2 = \frac{\sin \frac{\gamma_2}{2}}{2} \left[\frac{B}{n_2} + An_2 \right]$$

$$V_1 \cos(\alpha_1 + \beta) = V_2 \cos(\alpha_2 + \beta)$$

After considerable manipulation these equations reduce to the following

$$(1 + \frac{K}{Z}) = \cos \alpha_1 + \frac{F}{D} \sin \alpha_1 \quad (21)$$

$$\tan \alpha_2 = \frac{E}{G + \frac{D(1 + \frac{K}{Z})}{\sin \alpha_1}} \quad (22)$$

$$\frac{V_2}{V_1} = \frac{E}{D} \frac{\sin \alpha_1}{\sin \alpha_2} \quad (23)$$

where

$$D = \left[\frac{n_1}{n_2} + \frac{n_2}{n_1} \right] \sin \frac{\gamma_1}{2} \cos \frac{\gamma_2}{2} - \sin \gamma_1 - \left[\frac{n_1}{n_2} - \frac{n_2}{n_1} \right] \sin \frac{\gamma_1}{2} \sin \frac{\gamma_2}{2} \tan \beta$$

$$E = \sin \gamma_2 - \left[\frac{n_1}{n_2} + \frac{n_2}{n_1} \right] \cos \frac{\gamma_1}{2} \sin \frac{\gamma_2}{2} - \left[\frac{n_1}{n_2} - \frac{n_2}{n_1} \right] \sin \frac{\gamma_1}{2} \sin \frac{\gamma_2}{2} \tan \beta$$

$$F = \left[\frac{n_1}{n_2} - \frac{n_2}{n_1} \right] \cos \frac{\gamma_1}{2} \cos \frac{\gamma_2}{2} + \sin \gamma_1 \tan \beta - \left[\frac{n_1}{n_2} + \frac{n_2}{n_1} \right] \cos \frac{\gamma_1}{2} \sin \frac{\gamma_2}{2} \tan \beta$$

$$G = \sin \gamma_2 \tan \beta - \left[\frac{n_1}{n_2} - \frac{n_2}{n_1} \right] \cos \frac{\gamma_1}{2} \cos \frac{\gamma_2}{2} - \left[\frac{n_1}{n_2} + \frac{n_2}{n_1} \right] \sin \frac{\gamma_1}{2} \cos \frac{\gamma_2}{2} \tan \beta$$

Equation (21) gives us a relation between the cavitation number and the cavity length l_c . If we consider the limit as the solidity tends to infinity, this equation reduces to the expression obtained by Acosta and Hollander,⁽⁶⁾ for the case of semi-infinite flat plates. Further details are given in Appendix 1.

We now calculate the lift force acting on the hydrofoil. As mentioned previously, we will here adopt a slightly different perturbation procedure, so that a comparison may be made with the fully wetted case. We use the vector mean velocity V_m as reference velocity.

The element of force acting on the blade is

$$dF = (p - p_m) dx$$

$$\therefore F = \oint_{\text{body}} (p - p_m) dx$$

Defining the pressure coefficient c_p as

$$c_p = \frac{p - p_m}{\frac{1}{2} \rho V_m^2} \quad (24)$$

and the lift coefficient as

$$C_L = \frac{F}{\frac{1}{2} \rho V_m^2 c} \quad (24a)$$

we obtain

$$C_L = \frac{1}{c} \oint_{\text{body}} c_p dx$$

Using Bernoulli's equation this becomes

$$C_L = -\frac{1}{c} \oint_{\text{body}} \frac{2}{V_m} (u - V_m) dx$$

which reduces to

$$C_L = -\frac{2}{cV_m} \operatorname{Re} \operatorname{pt} \oint_{\text{body}} w(z) dz$$

on the body. Carrying out the indicated procedure in an identical way as previously performed for the closure condition we obtain

$$C_L = \frac{2}{cV_m} \left[V_1 \sin(\alpha_1 + \beta) - V_2 \sin(\alpha_2 + \beta) \right]$$

By the use of equations (5), (20) and (23), we can eliminate α_1 and α_2 in the above expression, and deduce the following:

$$C_L = \frac{4}{c} \frac{1}{\cos \beta} \left[\frac{\frac{D}{E} - 1}{\frac{D}{E} + 1} \right] \sin \alpha_m \quad (25)$$

As D, E are functions of l , the cavity length in the ζ -plane, this expression can be used to obtain the limiting case for the fully wetted cascade, i.e., when l tends to zero. This is carried out in Appendix II. The result reduces to that of the well known, fully wetted solution, viz.,

$$C_L = \frac{4}{\sigma} \frac{1}{\cos \beta} \left[\frac{a-1}{a+1} \right] \sin \alpha_m \quad (26)$$

A further limiting assumption in the linearized theory is that the angle of attack α_1 , is small. If second order powers of α are neglected, equations (21), (22), (23), and (24) reduce to

$$\frac{K}{2\alpha_1} = \frac{F}{D} \quad (21a)$$

$$\alpha_2 = \frac{E}{G + \frac{D}{\alpha_1} \left(1 + \frac{K}{2}\right)} \quad (22a)$$

$$V_2/V_1 = \frac{E}{D} \cdot \frac{\alpha_1}{\alpha_2} \quad (23a)$$

$$C_L = \frac{4}{\sigma} \frac{1}{\cos \beta} \left[\frac{\frac{D}{E} - 1}{\frac{D}{E} + 1} \right] \alpha_m \quad (25a)$$

From these equations, the results shown in Figures 6 - 28 were obtained.

V. Computational Procedure

The numerical calculations were conducted on a computer and the general method of computation is outlined below.

For a given cascade geometry, viz., σ and β , the value of a and ϕ were determined by the simultaneous numerical solution of equations (10) and (12). With these values, the functions D, E, F, and G were evaluated, for values of l , ranging from zero to

approximately two hundred; this latter figure giving a value of 0.99 for l_c/c . The ratio l_c/c can be found from equation (13). Having determined these quantities, the values of $K/2\alpha_1$, α_2 , V_2/V_1 and C_L are found for various angles of attack α_1 . The process is repeated for various stagger angles β , holding σ constant. This final parameter σ is then varied and the above procedure repeated. The range of values considered is given below in Table 1.

Parameter	Range
Solidity	0.25 to 1.25
Stagger angle	-75° to $+75^\circ$
Angle of attack	1° to 6°

Table 1

The Fortran program used in the computation of the results is given in Appendix III. This program is incorporated so that, if required, the data may be extended for other values of the parameters.

The data cards for the program have a format as given by statements 14 and 15. Statements 133 through 100 give the numerical method adopted for the simultaneous solution of equations (10) and (12) to obtain a and ϕ . The remainder of the program deals with the evaluation of the required data.

It should be noted that for the case of $\beta = 0$, the numerical solution adopted for the solution of equations (10) and (12) breaks down, and the program has to be slightly modified to accommodate this case. For $\beta = 0$, the above equations can be solved explicitly, hence statements 133 through 100 may be omitted. The remainder of the program is essentially the same though somewhat simplified.

VI. Discussion of Results

Figures 6 - 10 illustrate the relation between the cavity length and the cavitation number, for various geometries. The case of the isolated, partially cavitating flat plate is also shown on each graph. The values for this case were obtained from reference (9). It is of interest to note that a feature of the linearized theory is the fact that after a certain value of l_c/c the theory predicts two different cavity lengths for each cavitation number. This is apparent from figures 6 - 10. Since, in any case, the linearized assumption that the cavity-hydrofoil system forms a slender body would not be met for large values of l_c/c , it is assumed that the validity of the theory only holds good for values of $l_c/c < l_c/c$ minimum.

This behavior is to be expected due to the cavity model chosen, which places a singularity at the end of the cavity. However, comparing the results with that of the isolated hydrofoil, we see that this range of validity is increased in the case of the cascade. It would seem that the cascade effect has the property of reducing the strength of the singular behavior at the cavity end. This is further illustrated by the fact that as the solidity increases the range is extended, until at solidities greater than 0.75, a single valued function is obtained over almost the entire chord length for positive values of stagger angle. In the case of negative stagger angles, corresponding to the case of a turbine, as distinct from positive values of β which correspond to a pump, we see that there is still a region where the function is double valued. Physically, this is to be expected, since the effect of the neighboring blades is now no longer as effective near the cavity end.

It is seen that there is a large difference between the cavity geometry in cascade, compared with that of the isolated case, even for small solidities. However, this comparison is not entirely justified as the value of $K/2\alpha_1$ is based on the upstream angle of incidence. In the case of the cascade, a more natural angle to adopt is that of the mean velocity vector V_m .

Further, the curves at first glance seem to indicate that the cavity length for a given cavitation number at negative stagger angles is less than that of an isolated hydrofoil, even at low solidity. This surprising effect, however, is due once again to the choice of the upstream conditions as a reference. If the mean conditions are taken as reference, the curves for negative stagger angles will be raised above that for the isolated case and those corresponding to positive stagger angles remain below it as would be expected. If the curves are based on this angle, therefore, a better comparison is achieved. This is clearly illustrated in Figures 11 and 12 where the cavitation number is referred to the mean angle α_m .

There is still a significant difference for all values of β having solidities of 0.5 and greater. It therefore seems that the cascade effect is not very pronounced for solidities up to 0.5 provided the stagger angle is within the range -30° to $+60^\circ$.

Figures 13 and 14 illustrate a further representation. Here the value of $K_m/2\alpha_m$ is plotted against l_c/c , where K_m is defined as

$$K_m = \frac{P_m - P_c}{\frac{1}{2} \rho V_m^2}$$

which to first order, reduces to

$$K_m = K + (1+K)(\alpha_1 - \alpha_2)\tan \beta$$

with the help of Bernoulli's equation.

It is seen from these graphs, that for low solidity the curves lie very close to that of the isolated case, for all values of β . This representation, however, indicates the opposite effect to that using $K/2\alpha_1$, viz., that cavity lengths, for constant cavitation number, are longer for positive stagger angles than the isolated hydrofoil, even at low solidity. Consequently, it seems that the parameter $K/2\alpha_m$ is the most natural one to use.

A disadvantage of using these alternative forms is the fact that they depend on α_1 , whereas the value of $K/2\alpha_1$ is independent of the angle of attack α_1 and thus facilitates presentation immensely.

Figures 15 to 22 show the variation of force coefficient with cavitation number for varying cascade geometry. It is significant that the force coefficient is little changed over the range $-30^\circ < \beta < +30^\circ$ for a constant solidity. Since the linearized theory breaks down for large stagger angles, this effect is to be expected. The breakdown of the linearized theory is due largely to the fact that at large stagger angles the assumption that the cavity thickness is small compared with blade spacing can no longer be expected to hold, except for very small angles of attack. As shown in the curve, the force coefficient for the isolated hydrofoil is approached as the solidity decreases. However, once again, we see that for solidities of 0.5 and larger, the cascade effect is prominent.

The curves as plotted, are terminated at the points where l_c/c is a minimum. Here again, the point is illustrated that the mean conditions seem to be the natural choice for reference.

In the remaining curves, Figures 23 to 28, the behavior of the downstream conditions is illustrated. Here again, the curves are terminated at the point of minimum l_c/c . It may be pointed out that at $\beta = 0^\circ$ the theory gives V_2/V_1 as unity, but shows that α_2 is still variable and not equal to α_1 . This apparently is a violation of the continuity equation which would necessitate $\alpha_1 = \alpha_2$. This discrepancy is due to the linearization procedure which neglects quadratic terms.

VII. Conclusion

A linearized theory has been presented for the partial cavitation in a cascade of flat plates. The results have been presented in such a way that they may be useful as a guide in the design of turbo-machines and other applications. From the results, it is possible to determine the cavity length, lift coefficient and downstream conditions for any desired cavitation condition for a given specific cascade geometry and initial upstream conditions.

The limitations of the theory are stressed and it is shown that the cascade effect diminishes the singular behavior at the end of the cavity. In the case of the isolated foil the theory holds good up to a ratio of cavity length to chord length of approximately 0.74, whereas in the cascade flow this ratio varies from about 0.8 for small solidities up to 0.95 for larger solidities.

It is further shown that for solidities of 0.5 and over, the cascade effect is appreciable and cascade interference effects cannot be neglected in this range. However, for solidities smaller than 0.5 the cascade effect is relatively small and the isolated case may be used as a fairly good approximation provided that the mean conditions are taken as reference quantities.

Appendix I

From equations (10) and (12) we get

$$\tan \varphi = \frac{a-1}{a+1} \tan \beta$$

$$\sigma = \frac{1}{\pi} \cos \beta \ln a + \frac{2\varphi}{\pi} \sin \beta$$

hence

$$a = e^{\frac{\sigma \pi}{\cos \beta} - 2\varphi \tan \beta}$$

for

$$\sigma \rightarrow \infty \quad a \rightarrow \infty, \quad \varphi \rightarrow \beta$$

hence

$$n_1 \rightarrow [1 + l^2 - 2l \sin \beta]^{1/4}$$

$$\tan \psi_1 \rightarrow \frac{l \cos \beta}{1 - l \sin \beta}$$

$$n_2 \rightarrow 1$$

$$\psi_2 \rightarrow 0.$$

Therefore we get that

$$\sin \psi_1 = \frac{l \cos \beta}{n_1^2}$$

$$\cos \psi_1 = \frac{1 - l \sin \beta}{n_1^2}$$

and

$$\sin \frac{\psi_1}{2} = \frac{\sqrt{n_1^2 - 1 + l \cos \beta}}{\sqrt{2} n_1}$$

$$\cos \frac{\psi_1}{2} = \frac{\sqrt{n_1^2 + 1 - l \sin \beta}}{\sqrt{2} n_1}$$

Substituting in (21) gives

$$\left(1 + \frac{K}{2}\right) = \cos \alpha_1 + \sin \alpha_1 \frac{(n_1^2 - 1) \sqrt{n_1^2 + 1 - l \sin \beta} + \sqrt{2} l \sin \beta}{(n_1^2 + 1) \sqrt{n_1^2 - 1 + l \sin \beta} - \sqrt{2} l \cos \beta}$$

If we now change notation to that of Acosta and Hollander, we get

$$n_1 \equiv l \quad l \equiv b; \quad \beta \equiv \gamma; \quad \alpha_1 \equiv \alpha$$

and we further replace

$$\left(1 + \frac{K}{2}\right) \text{ by } \sqrt{1+K}$$

then

$$\sqrt{1+K} = \cos \alpha - \sin \alpha \frac{(1-l^2) \sqrt{l^2 + 1 - b \sin \gamma} - \sqrt{2} b \sin \gamma}{(1+l^2) \sqrt{l^2 - 1 + b \sin \gamma} - \sqrt{2} b \cos \gamma}$$

After some manipulation, this reduces to

$$\sqrt{1+K} = \cos \alpha - \sin \alpha \frac{b \cos \gamma}{l^2 - 1 + b \sin \gamma} \frac{(1-l^2) \cos \gamma - \sqrt{2} l \sqrt{1 - \frac{1-b \sin \gamma}{l^2}} \sin \gamma}{(1+l^2) \cos \gamma - \sqrt{2} l \sqrt{1 + \frac{1-b \sin \gamma}{l^2}} \cos \gamma}$$

which is the expression given by Acosta and Hollander.

Further, we see from equation (22) that since $E \rightarrow 0$ as

$\sigma \rightarrow \infty$ we get $\alpha_2 \equiv 0$ for all α_1 .

Appendix II

In the expressions for D and E we expand each term in powers of l , for small l , retaining powers up to and including $O(l^3)$

$$\left[\frac{n_1}{n_2} + \frac{n_2}{n_1} \right] \sim 2 + \left(\frac{1}{4} + \frac{1}{2a} + \frac{1}{4a^2} \right) \sin^2 \varphi l^2 + O(l^4)$$

$$\left[\frac{n_1}{n_2} - \frac{n_2}{n_1} \right] \sim -\left(1 + \frac{1}{a}\right) \sin \varphi l + \left(\frac{1}{2} - \sin^2 \varphi\right) \left(1 - \frac{1}{2a}\right) l^2 + O(l^3)$$

$$\sin \psi_1 \sim \cos \varphi l + \sin \varphi \cos \varphi l^2 - \left(\frac{\cos^2 \varphi}{2} - \sin^2 \varphi\right) \cos \varphi l^3 + O(l^4)$$

$$\sin \psi_2 \sim \frac{\cos \varphi}{a} l - \frac{\sin \varphi \cos \varphi}{a^2} l^2 - \left(\frac{\cos^2 \varphi}{2} - \sin^2 \varphi\right) \frac{\cos \varphi}{a^3} l^3 + O(l^4)$$

$$\sin \frac{\psi_1}{2} \cos \frac{\psi_2}{2} \sim \frac{\cos \varphi}{2} l + \frac{\sin \varphi \cos \varphi}{2} l^2 + \left(\sin^2 \varphi - \frac{3}{8} \cos^2 \varphi - \frac{\cos^2 \varphi}{8a}\right) \frac{\cos \varphi}{2} l^3 + O(l^4)$$

$$\sin \frac{\psi_1}{2} \sin \frac{\psi_2}{2} \sim \frac{\cos^2 \varphi}{4a} l^2 + \left(1 - \frac{1}{a}\right) \frac{\sin \varphi \cos^2 \varphi}{4a} l^3 + O(l^4)$$

$$\cos \frac{\psi_1}{2} \sin \frac{\psi_2}{2} \sim \frac{\cos \varphi}{2a} l - \frac{\sin \varphi \cos \varphi}{2a^2} l^2 - \left(\frac{\cos^2 \varphi}{8} + \frac{3 \cos^2 \varphi}{8a^2} - \frac{\sin^2 \varphi}{a^2}\right) \frac{\cos \varphi}{2a} l^3 + O(l^4)$$

Utilizing these expressions we obtain

$$D = \left[\left(\frac{1}{8} + \frac{1}{4a} + \frac{1}{8a^2}\right) \sin^2 \varphi \cos \varphi + \left(\frac{1}{8} - \frac{1}{8a^2}\right) \cos^3 \varphi + \left(1 + \frac{1}{a}\right) \frac{1}{4a} \sin \varphi \cos^2 \varphi \tan \beta \right] l^3 + O(l^4)$$

$$E = \left[-\left(\frac{1}{8a} + \frac{1}{4a^2} + \frac{1}{8a^3}\right) \sin^2 \varphi \cos \varphi + \left(\frac{1}{8a} - \frac{1}{8a^3}\right) \cos^3 \varphi + \left(1 + \frac{1}{a}\right) \frac{1}{4a} \sin \varphi \cos^2 \varphi \tan \beta \right] l^3 + O(l^4)$$

hence

$$\frac{D}{E} \sim a \frac{\left[\left(\frac{1}{8} + \frac{1}{4a} + \frac{1}{8a^2}\right) \sin^2 \varphi \cos \varphi + \left(\frac{1}{8} - \frac{1}{8a^2}\right) \cos^3 \varphi + \left(1 + \frac{1}{a}\right) \frac{1}{4a} \sin \varphi \cos^2 \varphi \tan \beta \right]}{\left[-\left(\frac{1}{8} + \frac{1}{4a} + \frac{1}{8a^2}\right) \sin^2 \varphi \cos \varphi + \left(\frac{1}{8} - \frac{1}{8a^2}\right) \cos^3 \varphi + \left(1 + \frac{1}{a}\right) \frac{1}{4} \sin \varphi \cos^2 \varphi \tan \beta \right]} + O(l)$$

Now substituting for $\tan \beta = \frac{a-1}{a+1} \tan \varphi$ in above, gives

$$\frac{D}{E} \sim a + O(l) \quad \text{as } l \rightarrow 0$$

thus

$$C_L = \frac{4}{\sigma} \frac{1}{\cos \beta} \left[\frac{a-1}{a+1} \right] \sin \alpha_m \quad \text{as } l \rightarrow 0$$

which is the classical fully wetted cascade flow result. Now, when

$\beta = 0$, $a = e^{\sigma\pi}$ then

$$C_L = 2\pi \frac{\tanh(\sigma\pi/2)}{(\sigma\pi/2)} \sin \alpha_m$$

for the isolated hydrofoil $\sigma \rightarrow 0$ this reduces to

$$C_L = 2\pi \alpha_m.$$

Appendix III

We present here the Fortran Source Program as used in the computation of the results presented in this report. The notation used is self evident from the program.

```
DIMENSION FLCP(500),ELCN(500),AP(500),AN(500),
XBP(500),FN(500),CP(500),CN(500),DP(500),DN(500)
5  FORMAT(1H )
14  FORMAT(4I5,F10.8)
15  FORMAT(4I10.8)
16  FORMAT(6L10.8)
20  FORMAT(8H SIGMA=E16.8,7H BETA=E16.8,
X3H A=E16.8,5H PHI=[16.8,7H ALPH1=E16.8)
30  FORMAT(1H ,F9.3,8F12.4,F8.4)
22  FORMAT(6X,1HL,8X,1HK,7X,8HK/2ALPH1,6X,4HALF2,
X9X,6HALF2/1,6X,5HV2/V1,9X,2HCL,6X,9HDCL/DALFM,
X8X,2HLC,4X,4HLC/C)
133  FORMAT(1H 8L12.4)
PAM1F(A,W1,W2)=W1-W2*LOGF(A)
PAM2F(A,W3)=ATANF((A-1.)*W3/(A+1.))
READ 14,NSIG,NBET,NAL,NEL,CONST
READ 15,SIGMO,DSIG,BETO,DBCT,ALPHO,DAL,AD,DAO,ELO,DEL
SIGMA=SIGMU
DO 5000 ISIG=1,NSIG
DICK=3.1415926*SIGMA*0.5
BETA=BETU
DO 4000 IBCT=1,NBET
W1=DICK/SINF(BETA)
W3=SINF(BLTA)/COSF(BETA)
W2=0.5/W3
A=AU
DA=DAU
40  Y1=PAM1F(A,W1,W2)
Y2=PAM2F(A,W3)
Y3=(Y1-Y2)/(Y1+Y2)
Y4=ARSF(Y3)
IF(Y3)50,100,60
50  IF(Y4-CONST)100,100,55
55  A=A-DA
DA=DA/10.
A=A+DA
GO TO 40
60  A=A+DA
GO TO 40
100  PHI=Y1
L=U
DO 3000 IEL=1,NEL
F1=IEL*IEL
EL=F1*DEL
F1=(1.+EL*EL)
F2=(1.+((EL/A)**2))
F3=2.*EL*SINF(PHI)
ENP14=F1-F3
ENP24=F2+(F3/A)
ENN14=F1+F3
ENN24=F2-(F3/A)
HAP=ENP14/ENP24
HAN=ENN14/ENN24
F1=EL*COSF(PHI)*(A-1.)
F2=EL*EL*SINF(2.*PHI)
F3=A+EL*FL*COSF(2.*PHI)
```

```
F4=(A-1.)*EL*SINF(PHI)
GPHA=- (F1+F2)/(F3-F4)
GNHA=- (F1-F2)/(F3+F4)
IF(PHI-0.75) 3010, 3010, 3020
3010 GAMP=ATANF(GPHA)
      GAMN=ATANF(GNHA)
      GO TO 3050
3020 IF(GNHA) 3021, 3021, 3022
3021 GAMN=ATANF(GNHA)
      GO TO 3028
3022 GAMN=ATANF(GNHA)+3.1415926
3028 IF(GPHA) 3030, 3030, 3029
3029 L=1
3030 IF(L) 3031, 3031, 3040
3031 GAMP=ATANF(GPHA)
      GO TO 3050
3040 IF(GPHA) 3045, 3042, 3042
3042 GAMP=ATANF(GPHA)
      GO TO 3050
3045 GAMP=ATANF(GPHA)+3.1415926
3050 ELCF(IEI)=COSF(BETA)*LOGF(HAP)-2.*SINF(BETA)*GAMP
      ELCN(IEI)=COSF(BETA)*LOGF(HAN)+2.*SINF(BETA)*GAMN
      F1=SQRTF(ENP14)
      ENP1=SQRTF(F1)
      F1=SQRTF(FNP24)
      ENP2=SQRTF(F1)
      F1=SQRTF(ENN14)
      ENN1=SQRTF(F1)
      F1=SQRTF(ENN24)
      ENN2=SQRTF(F1)
      F1=EL*COSF(PHI)
      F2=EL*SINF(PHI)
      TP1=F1/(1.-F2)
      TP2=F1/(A+F2)
      TN1=F1/(1.+F2)
      TN2=F1/(A-F2)
      FP1=1./SQRTF(1.+TP1*TP1)
      FP2=1./SQRTF(1.+TP2*TP2)
      FN1=1./SQRTF(1.+TN1*TN1)
      FN2=1./SQRTF(1.+TN2*TN2)
      SP1=ABSF(TP1*FP1)
      SP2=ABSF(TP2*FP2)
      SN1=TN1*FN1
      SN2=ABSF(TN2*FN2)
      CP1=SIGNF(FP1, TP1)
      CP2=FP2
      CN1=FN1
      CN2=SIGNF(FN2, TN2)
      SPH1=SQRTF(0.5*(1.-CP1))
      SPH2=SQRTF(0.5*(1.-CP2))
      SNH1=SQRTF(0.5*(1.-CN1))
      SNH2=SQRTF(0.5*(1.-CN2))
      CPH1=SQRTF(0.5*(1.+CP1))
      CPH2=SQRTF(0.5*(1.+CP2))
      CNH1=SQRTF(0.5*(1.+CN1))
      CNH2=SQRTF(0.5*(1.+CN2))
```

```
FP1=ENP1/ENP2
FP2=1./FP1
FN1=ENN1/FNN2
FN2=1./FN1
FO=SINF(BETA)/COSF(BETA)
F1=FP1+FP2
F2=FP1-FP2
F3=SPH1*SPH2*F2*FO
F4=F1*FO
F5=F2*CPH1*CPH2
AP( IEL)=F1*SPH1*CPH2-SP1-F3
BP( IEL)=SP2-F1*SPH2*CPH1-F3
CP( IEL)=F5+SP1*FO-F1*CPH1*SPH2*FO
DP( IEL)=SP2*FO-F5-F1*SPH1*CPH2*FO
FO=-FO
F1=FN1+FN2
F2=FN1-FN2
F3=SNH1*SNH2*F2*FO
F4=F1*FO
F5=F2*CNH1*CNH2
AN( IEL)=F1*SNH1*CNH2-SN1-F3
BN( IEL)=SN2-F1*SNH2*CNH1-F3
CN( IEL)=F5+SN1*FO-F1*CNH1*SNH2*FO
3000 DN( IEL)=SN2*FO-F5-F1*SNH1*CNH2*FO
ALPH1=ALPH0
DO 3500 IAL=1,NAL
PRINT 5
PRINT 20,SIGMA,BETA,A,PHI,ALPH1
PRINT 5
PRINT 22
PRINT 5
DO 3150 IEL=1,NEL
F1=IEL*IEL
EL=F1*DCL
CAPO=CP( IEL)/AP( IEL)
CAPA=2.*ALPH1*CAPO
ALPH2=BP( IEL)/(DP( IEL)+(AP( IEL)*(1.+CAPA*0.5)/
(ALPH1))
ALPH21=ALPH2/ALPH1
V2V1=BP( IEL)/(AP( IEL)*ALPH21)
F1=AP( IEL)/BP( IEL)
DCL=4.*(F1-1.)/((F1+1.)*SIGMA*COSF(BETA))
F2=ALPH1+BETA
F4=SINF(F2)/COSF(F2)
F2=ALPH2+BETA
F5=SINF(F2)/COSF(F2)
F3=0.5*(F4+F5)
IF(F3)3105,3110,3110
3105 ALPHM=ATANF(F3)-BETA+3.1415926
GO TO 3115
3110 ALPHM=ATANF(F3)-BETA
3115 CLL=DCL*ALPHM
F1=ELCP( IEL)/(4.*DICK)
3150 PRINT 30,FL,CAPA,CAPO,ALPH2,ALPH21,V2V1,CLL,DCL,
XELCP( IEL),F1
PRINT 5
```

```
F1=-BETA
F2=-PHI
PRINT 20,SIGMA,F1,A,F2,ALPH1
PRINT 5
PRINT 22
PRINT 5
DO 3250 ILL=1,NEL
F1=ILL*IEL
EL=F1*DEL
CAPD=CN(IFL)/AN(IEL)
CAPA=2.*CAPD*ALPH1
ALPH2=BN(IEL)/(DN(IEL)+(AN(IEL)*(1.+CAPA*0.5)/
XALPH1))
ALPH21=ALPH2/ALPH1
V2V1=BN(IEL)/(AN(IFL)*ALPH21)
F1=AN(IEL)/BN(IEL)
DCL=4.*(F1-1.)/((F1+1.)*SIGMA*COSF(BETA))
F2=ALPH1-BETA
F4=SINF(F2)/COSF(F2)
F2=ALPH2-BLTA
F5=SINF(F2)/COSF(F2)
F3=0.5*(F4+F5)
IF(F3)3210,3210,3205
3205 ALPHM=ATANF(F3)+BETA-3.1415926
GO TO 3215
3210 ALPHM=ATANF(F3)+BETA
3215 CLL=DCL*ALPHM
F1=ELCN(IEL)/(4.*DICK)
3250 PRINT 30,EL,CAPA,CAPD,ALPH2,ALPH21,V2V1,CLL,DCL,
XELCN(IEL),F1
3500 ALPH1=ALPH1+DAL
4000 BETA=BETA+DBET
5000 SIGMA=SIGMA+DSIG
CALL EXII
END
```

REFERENCES

1. Garrick, I. E., "On the Plane Potential Flow Past a Lattice of Arbitrary Airfoils." NACA Report No. 788, 1944.
2. Robinson, A. and Laurmann, J. A., "Wing Theory". Cambridge University Press, Cambridge, England. 1956.
3. Tulin, M. P., "Steady Two-Dimensional Cavity Flows About Slender Bodies." David Tyler Model Basin Rep. 834, May 1953.
4. Parkin, B. R., "Linearized Theory of Cavity Flow in Two-Dimensions." Rep. P-1745, Rand Corporation, Santa Monica, California.
5. Cohen, H. and Sutherland, C. D., "Finite Cavity Cascade Flow." Math. Rep. No. 14, Rensselaer Polytechnic Institute, Troy, New York, April 1958.
6. Acosta, A. J. and Hollander, A., "Remarks on Cavitation in Turbomachines." Rep. No. 79-3, Eng. Div., California Institute of Technology, Pasadena, California, October 1959.
7. Stripling, L. B. and Acosta, A. J., "Cavitation in Turbo Pumps - Part 1." Transactions of the ASME, Journal of Basic Engineering, September 1962.
8. Acosta, A. J., "Cavitating Flow Past a Cascade of Circular Arc Hydrofoils." Rep. No. E-79-2, Eng. Div., California Institute of Technology, Pasadena, California, March 1950.
9. Acosta, A. J., "A Note on Partial Cavitation of Flat Plate Hydrofoils." Rep. No. E-19-9, Hydrodynamic Lab., California Institute of Technology, Pasadena, California, October 1955.

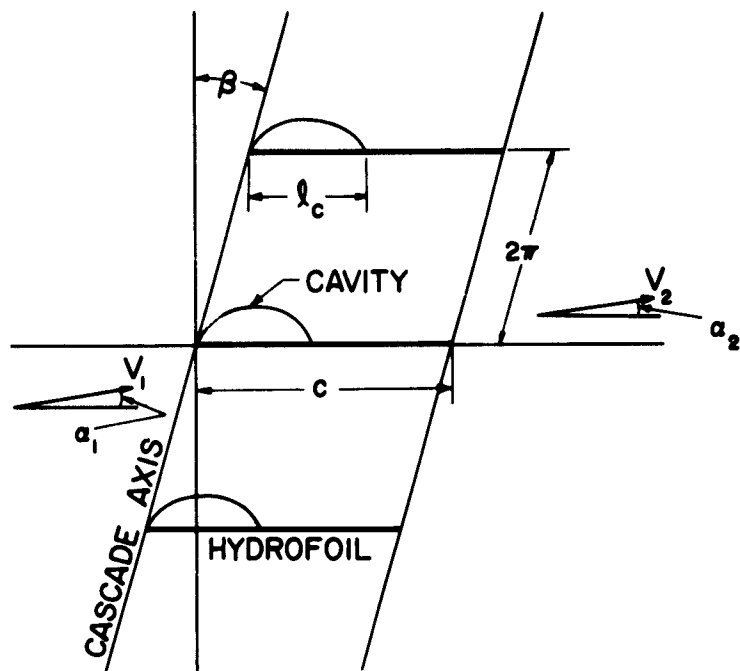


Fig. 1 Partially cavitating cascade of flat plates.

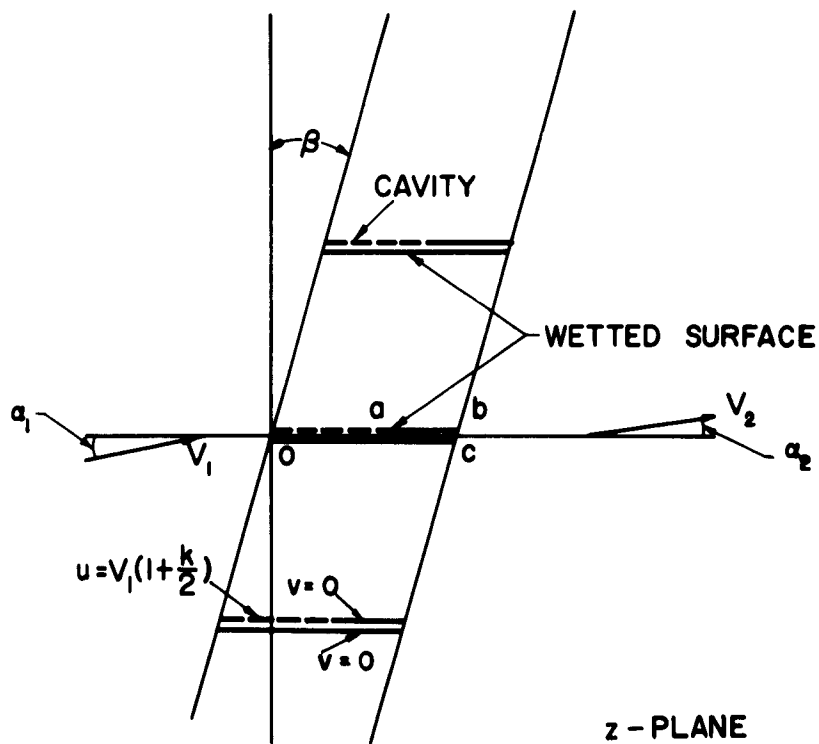


Fig. 2 Linearized boundary conditions in physical z-plane.

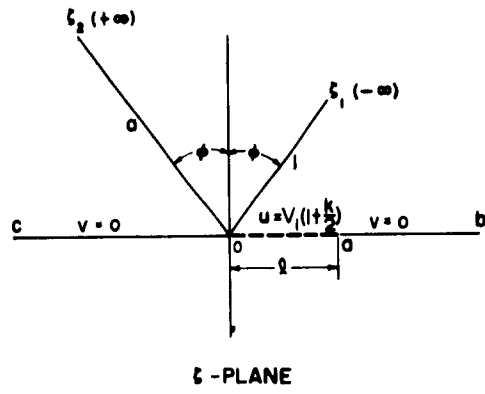


Fig. 3 Auxiliary ξ -plane.

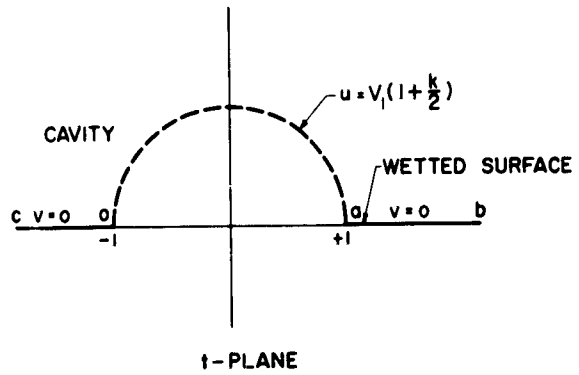


Fig. 4 Auxiliary t -plane.

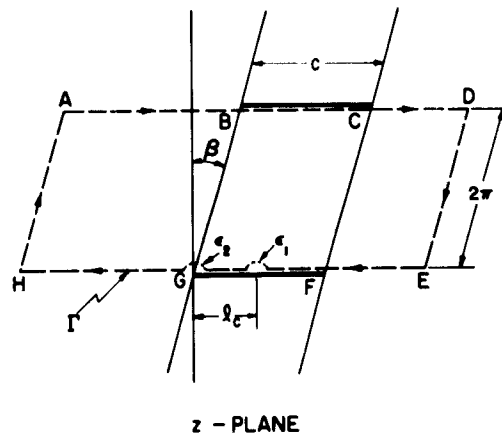


Fig. 5 Integration contour in z -plane.

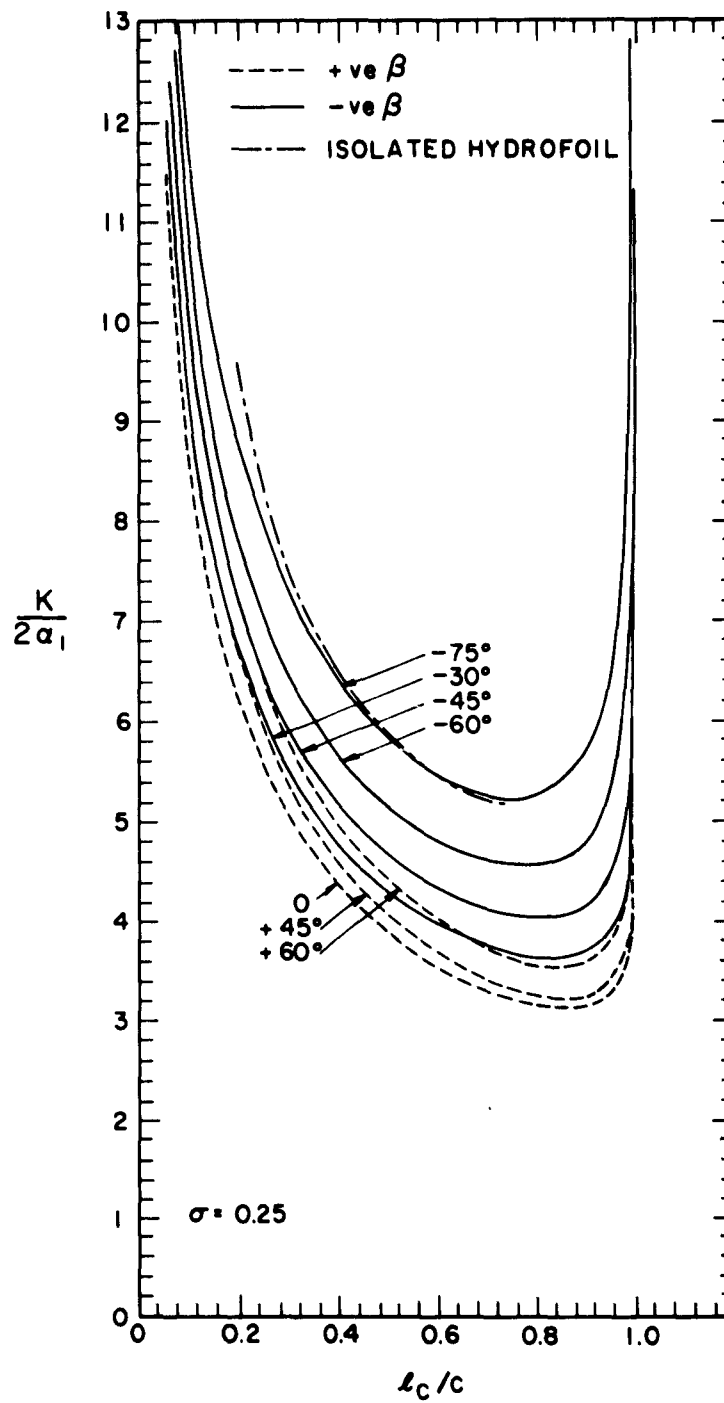


Fig. 6 Ratio of cavitation number to twice inlet angle vs. cavity length to chord length ratio for various stagger angles β , at a constant solidity, $\sigma = 0.25$.

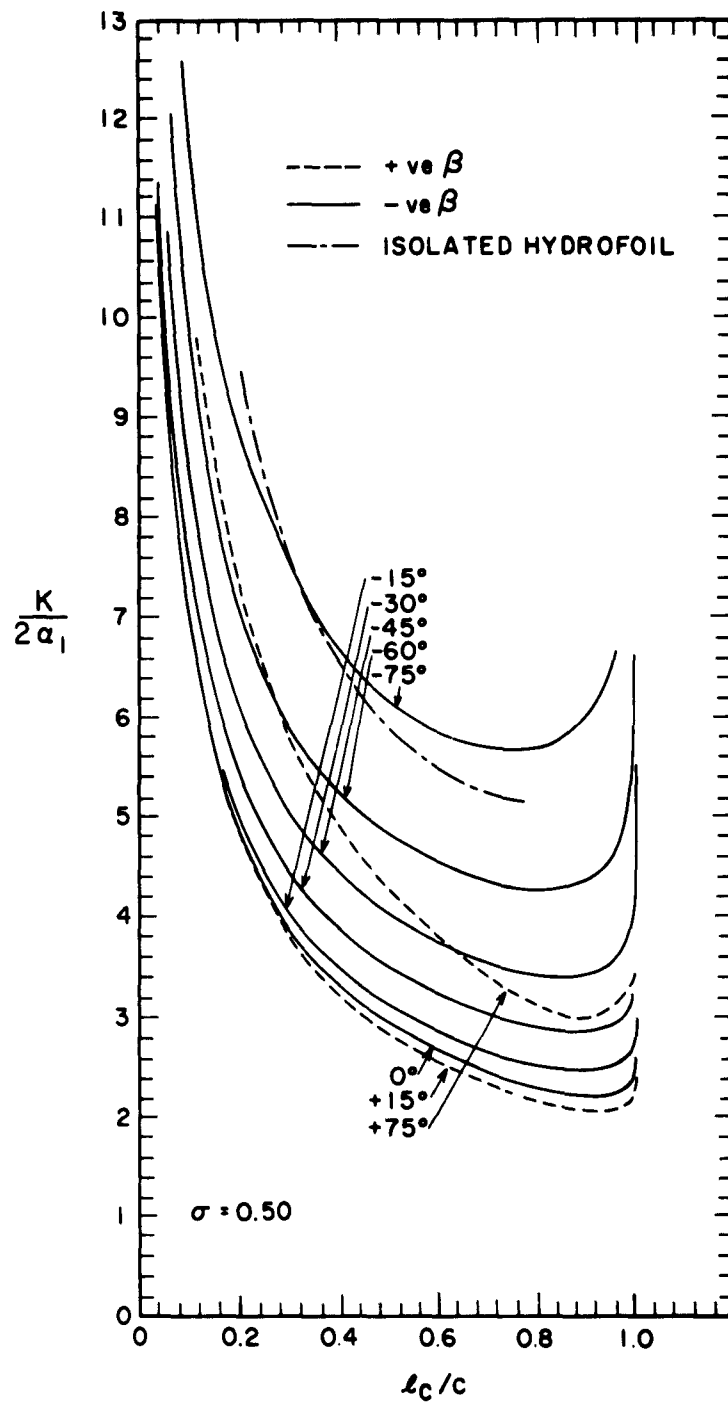


Fig. 7 Ratio of cavitation number to twice inlet angle vs. cavity length to chord length ratio for various stagger angles β , at a constant solidity, $\sigma = 0.50$.

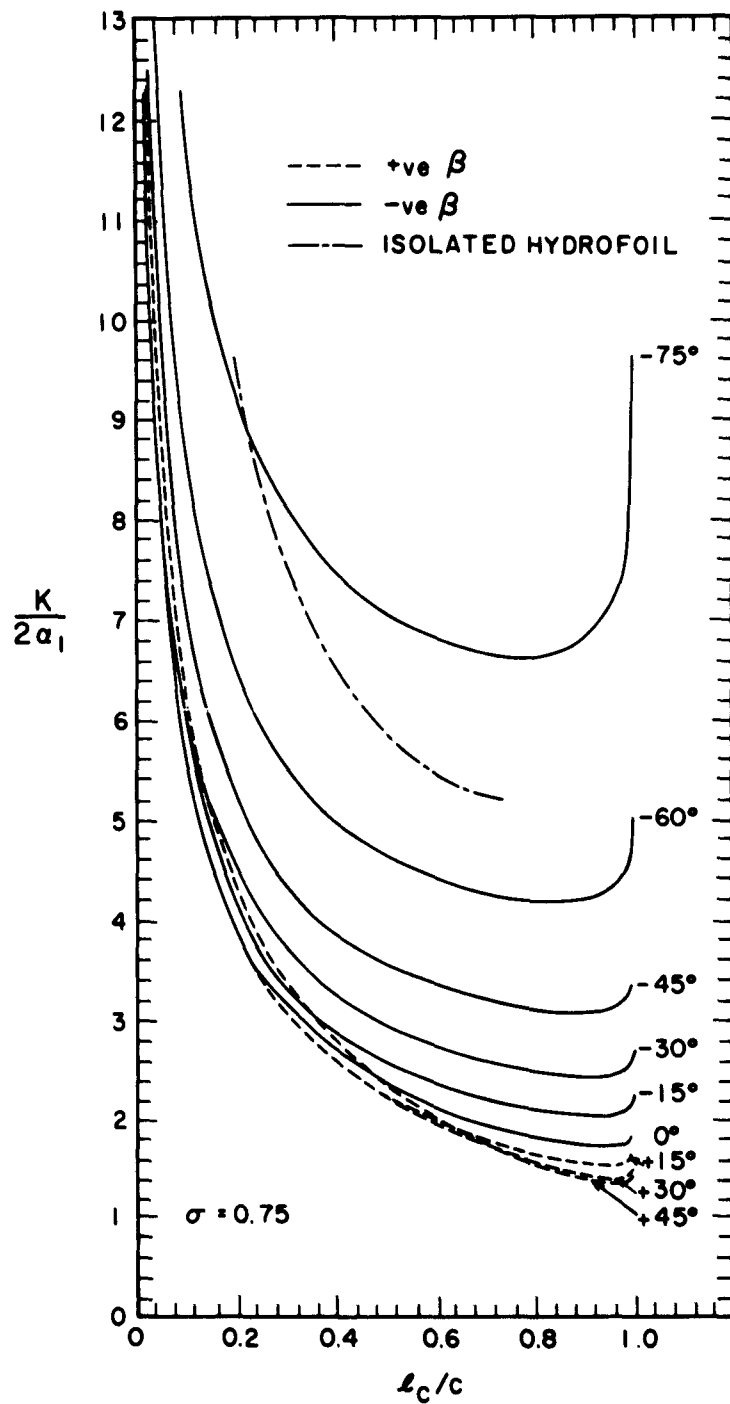


Fig. 8 Ratio of cavitation number to twice inlet angle vs. cavity length to chord length ratio for various stagger angles β , at a constant solidity, $\sigma = 0.75$.

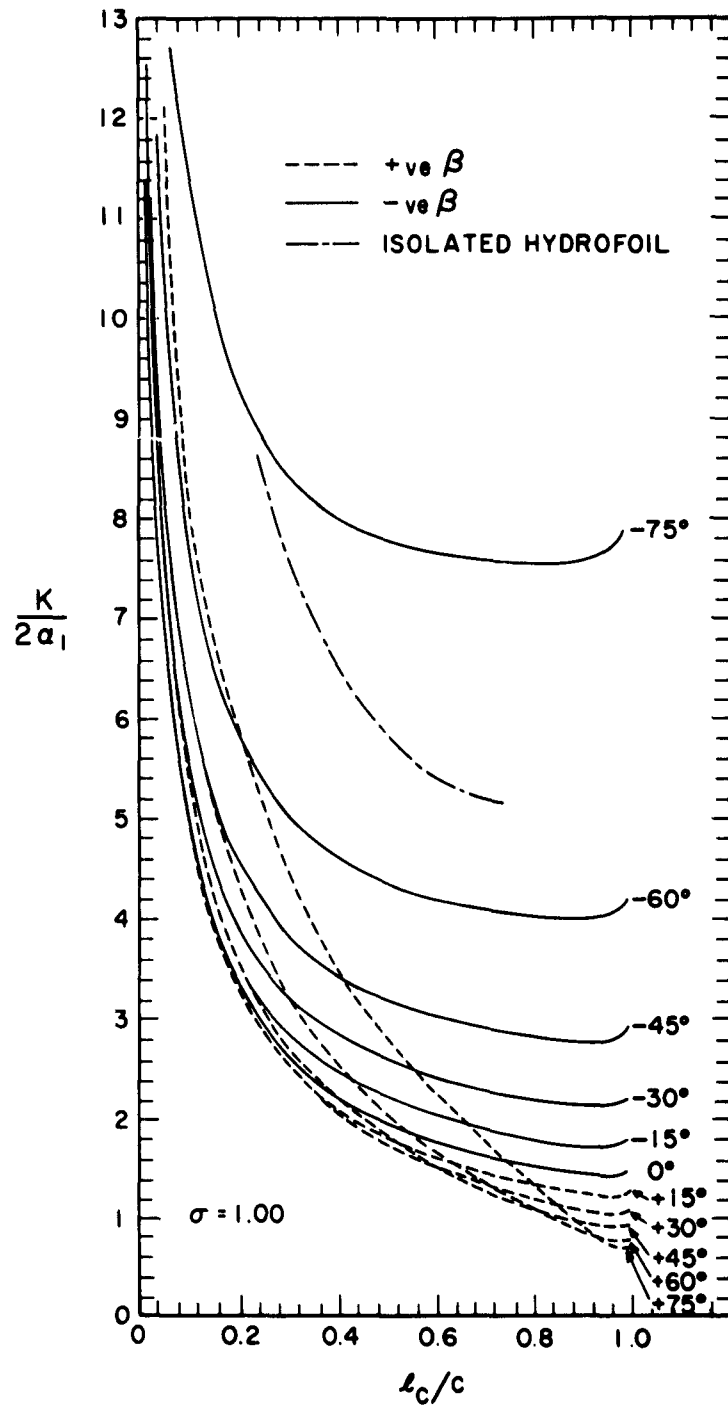


Fig. 9 Ratio of cavitation number to twice inlet angle vs. cavity length to chord length ratio for various stagger angles β , at a constant solidity, $\sigma = 1.00$

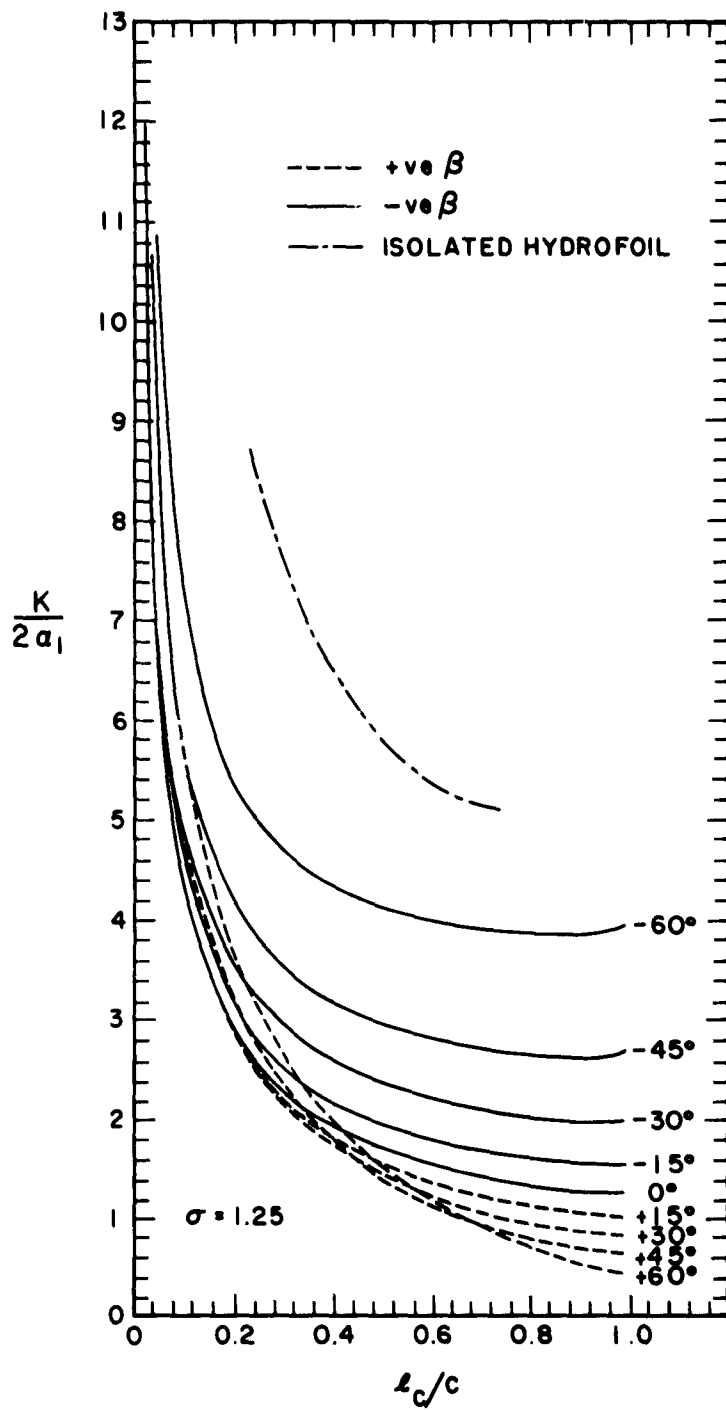


Fig. 10 Ratio of cavitation number to time inlet angle vs. cavity length to chord length ratio for various stagger angles β , at a constant solidity, $\sigma = 1.25$.

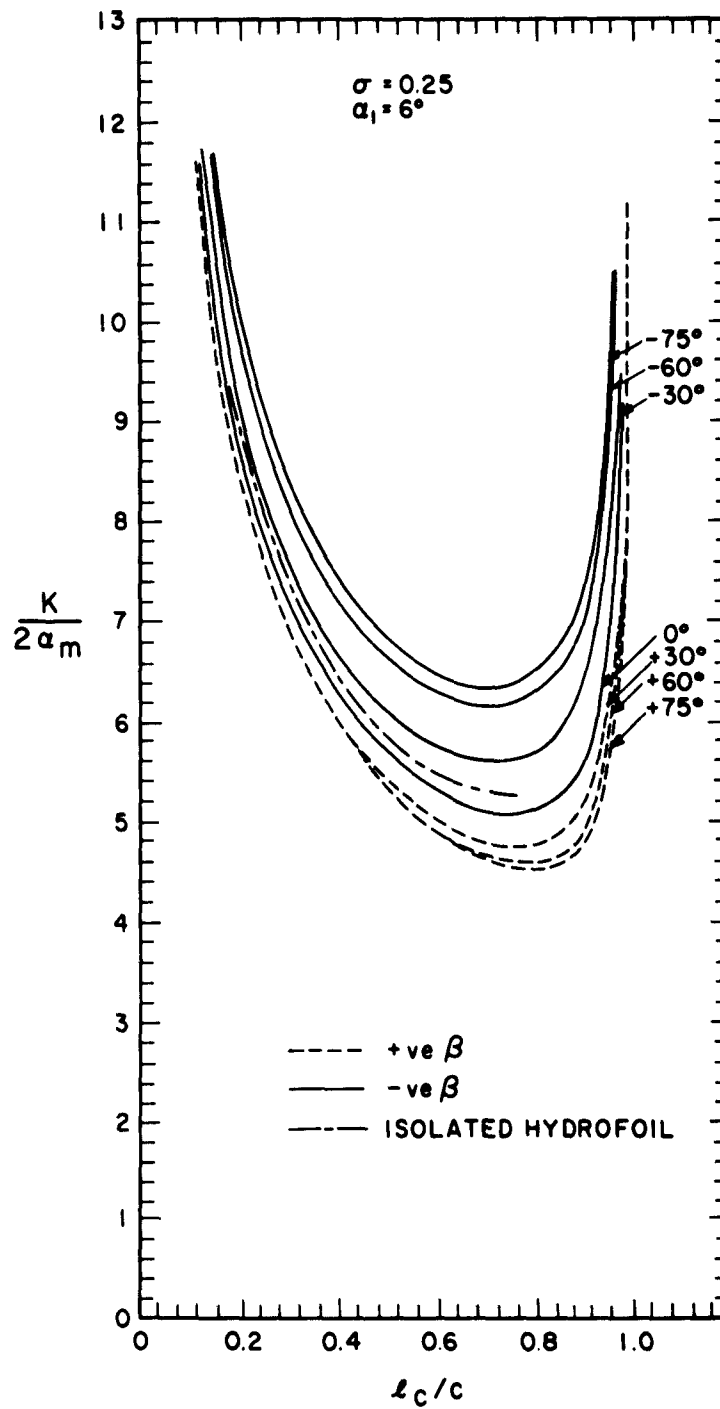


Fig. 11 Ratio of cavitation number to twice the mean flow angle vs. cavity length to chord length ratio for various stagger angles β , at a constant solidity $\sigma = 0.25$ and inlet angle of 6° .

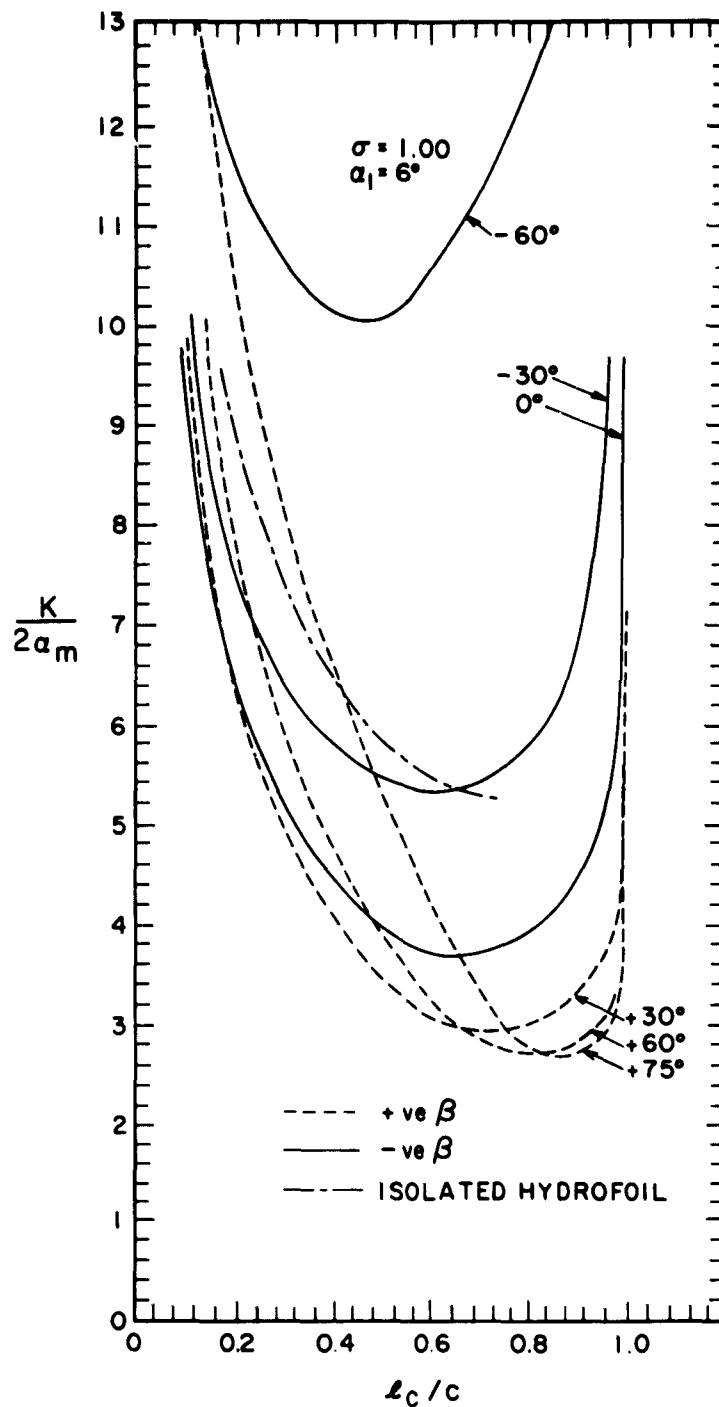


Fig. 12 Ratio of cavitation number to twice the mean flow angle vs. cavity length to chord length ratio for various stagger angles β , at a constant solidity $\sigma = 1.00$ and inlet angle of 6° .

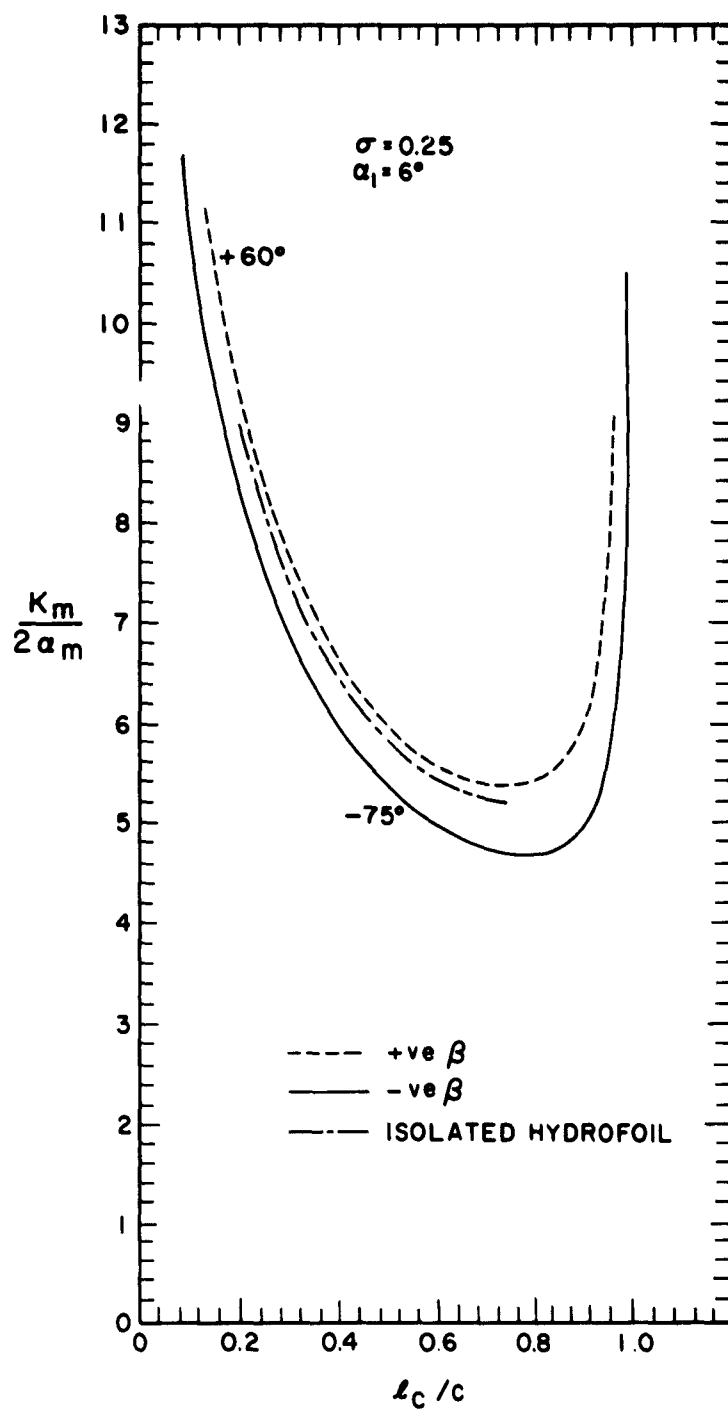


Fig. 13 Ratio of mean cavitation number to twice mean flow angle vs. cavity length to chord length ratio for various stagger angles β , at a constant solidity $\sigma = 0.25$ and inlet angle of 6° .

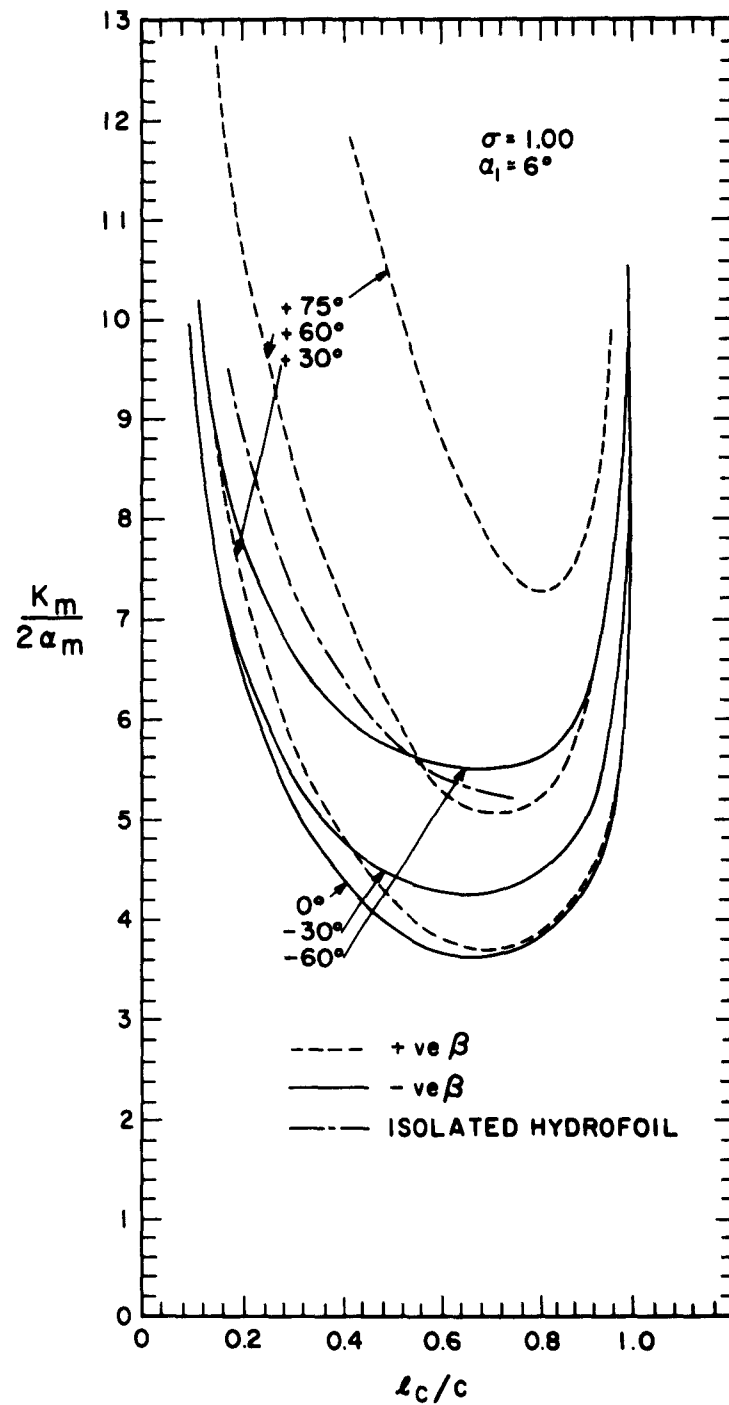


Fig. 14 Ratio of mean cavitation number to twice mean flow angle vs. cavity length to chord length ratio for various stagger angles β , at a constant solidity $\sigma = 1.00$ and inlet angle of 6° .

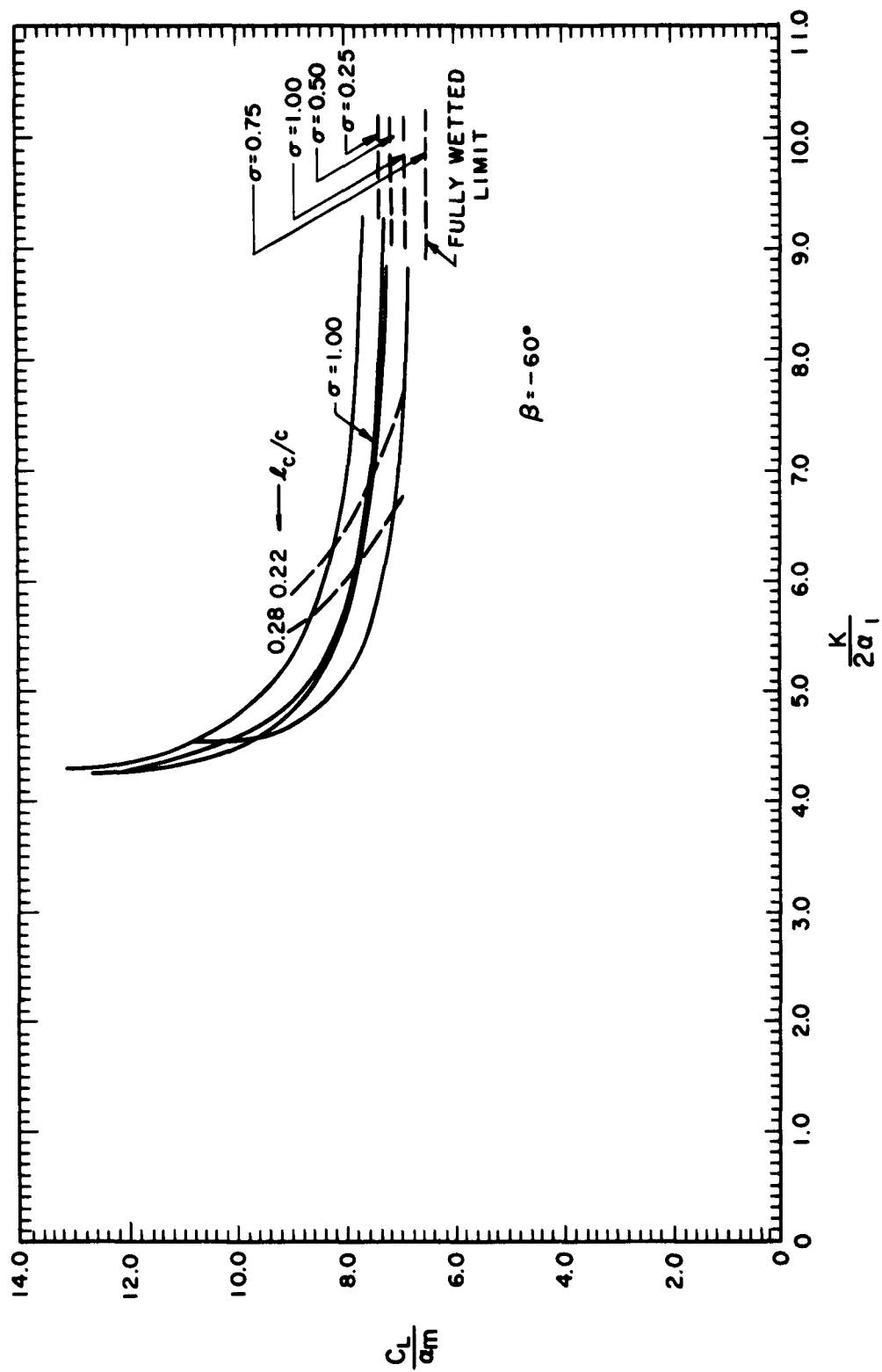


Fig. 15 Ratio of lift coefficient to mean flow angle vs. ratio of cavitation number to twice inlet angle for various solidities at a given stagger angle $\beta = -60^\circ$.

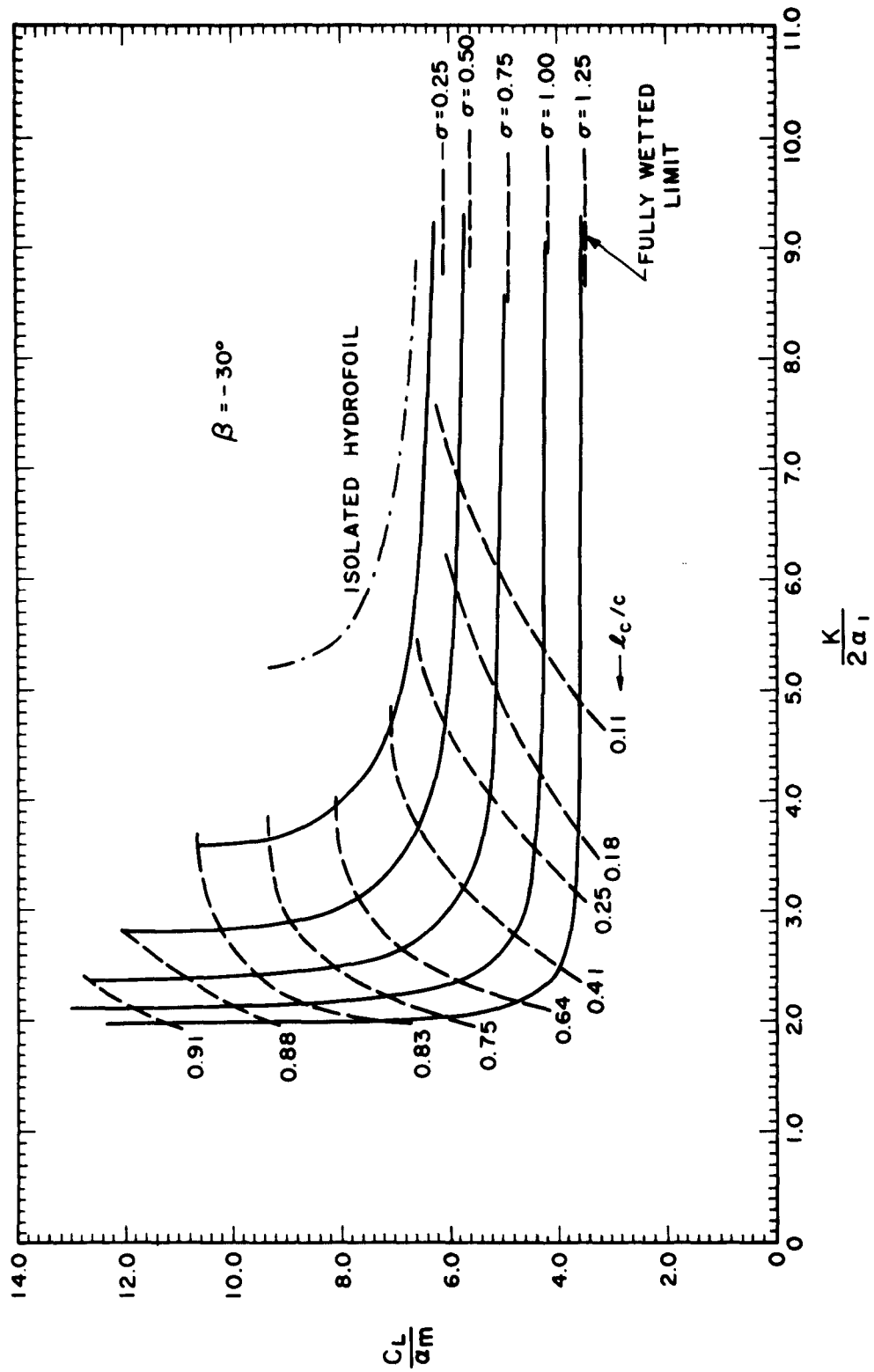


Fig. 16 Ratio of lift coefficient to mean flow angle vs. ratio of cavitation number to twice inlet angle for various solidities at a given stagger angle $\beta = -30^\circ$.

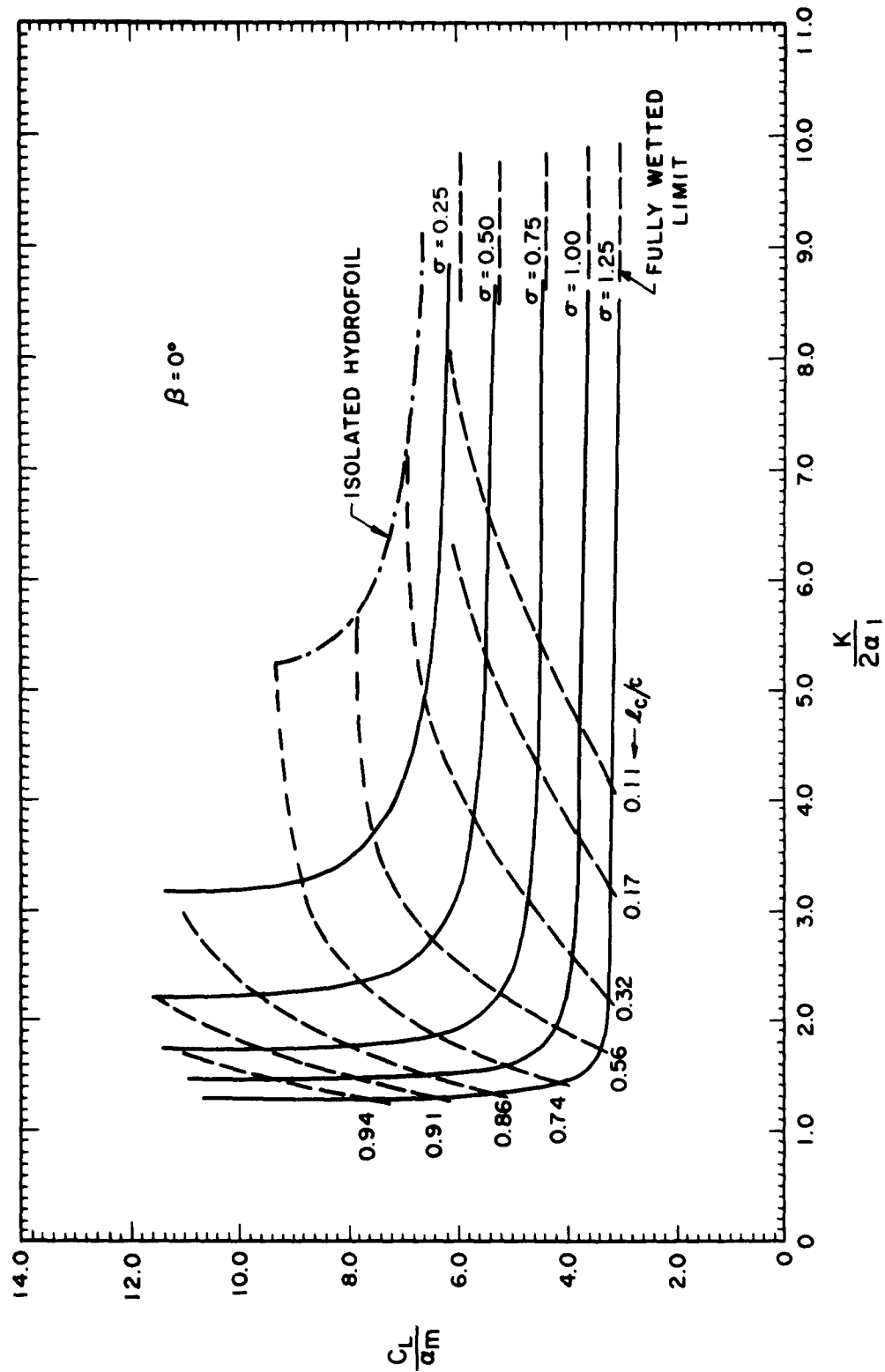


Fig. 17 Ratio of lift coefficient to mean flow angle vs. ratio of cavitation number to twice inlet angle for various solidities at a given stagger angle $\beta = 0^\circ$.

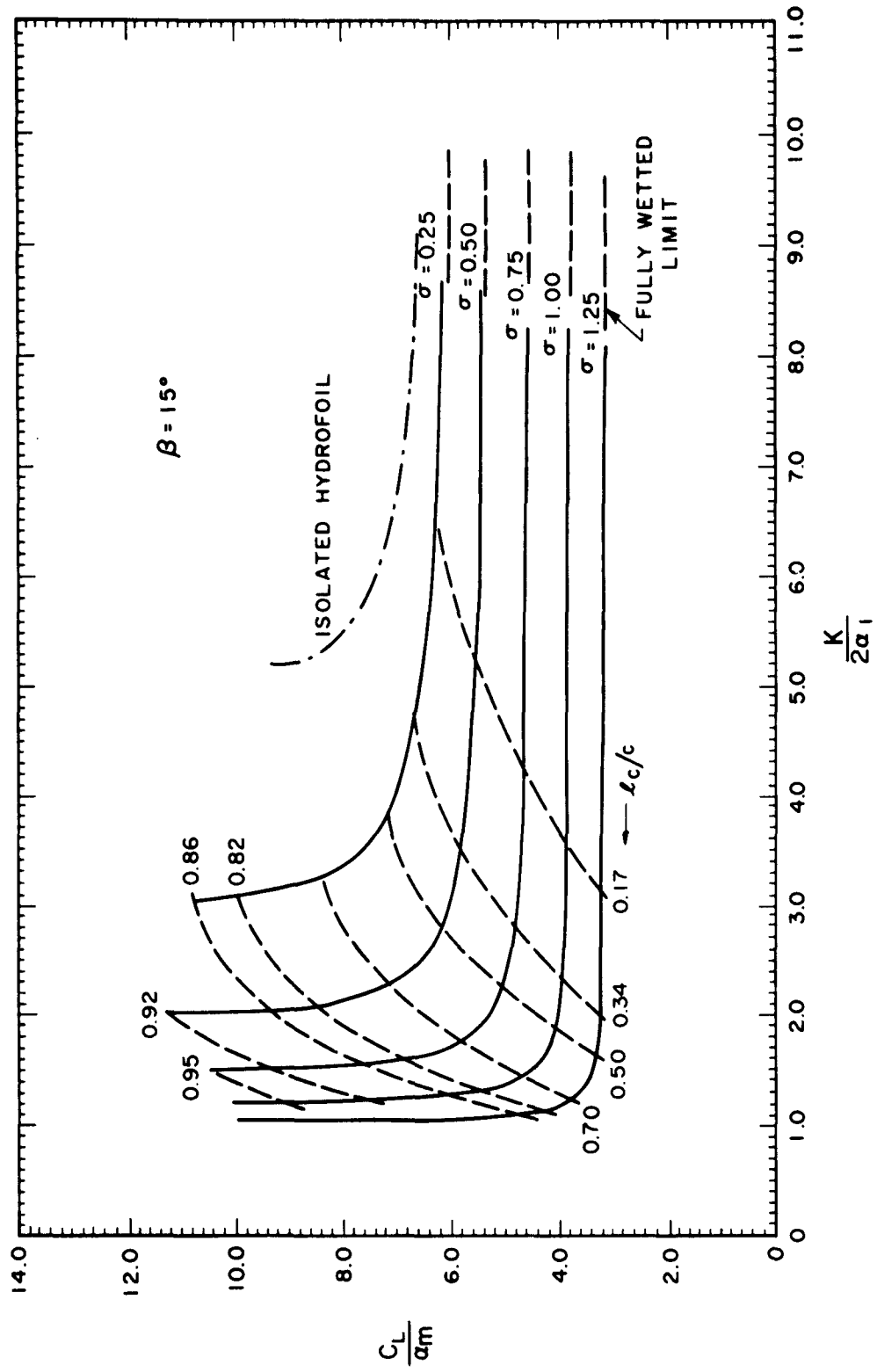


Fig. 18 Ratio of lift coefficient to mean flow angle vs. ratio of cavitation number to twice inlet angle for various solidities at a given stagger angle $\beta = 15^\circ$.

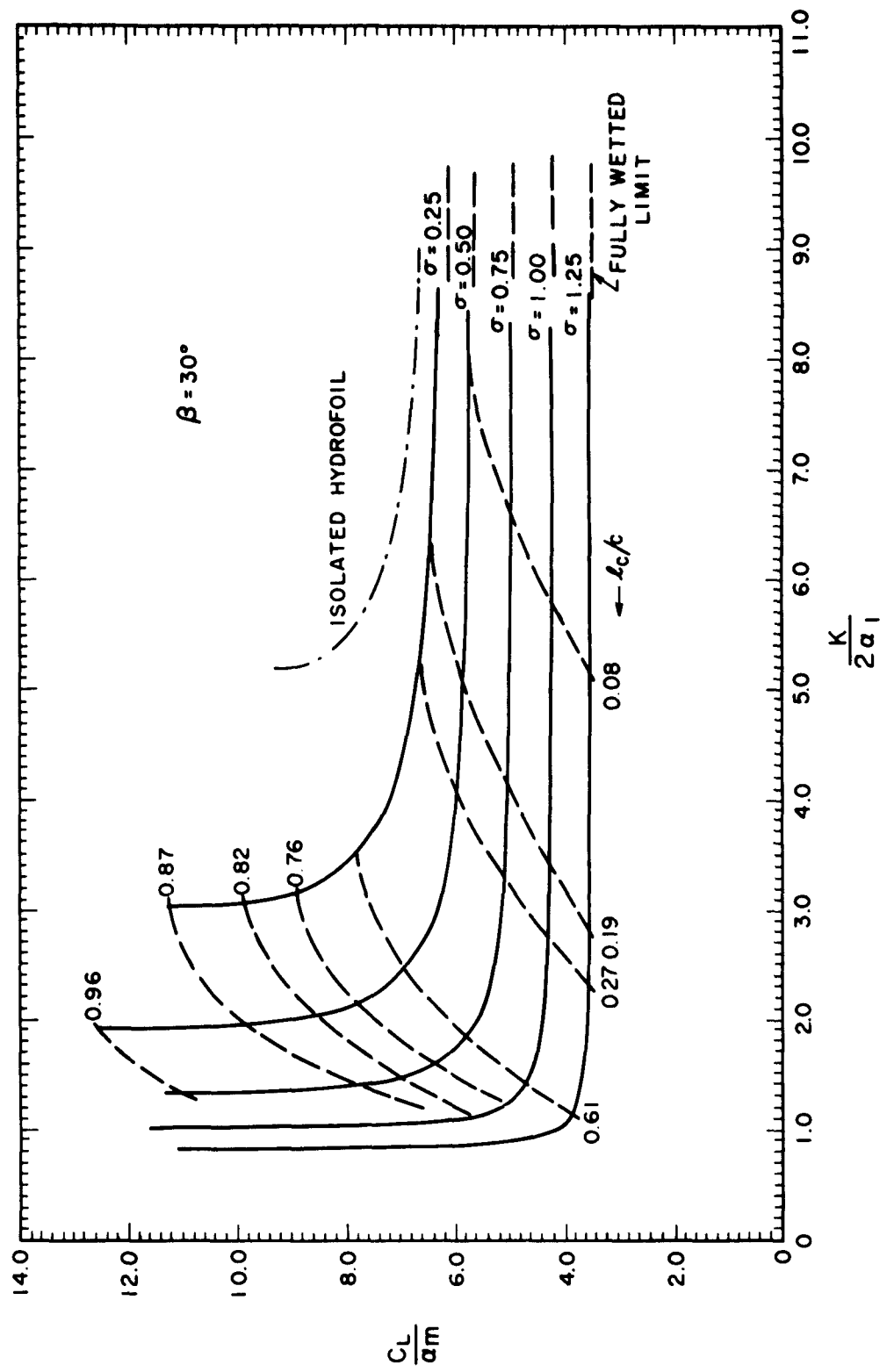


Fig. 19 Ratio of lift coefficient to mean flow angle vs. ratio of cavitation number to twice inlet angle for various solidities at a given stagger angle $\beta = 30^\circ$.

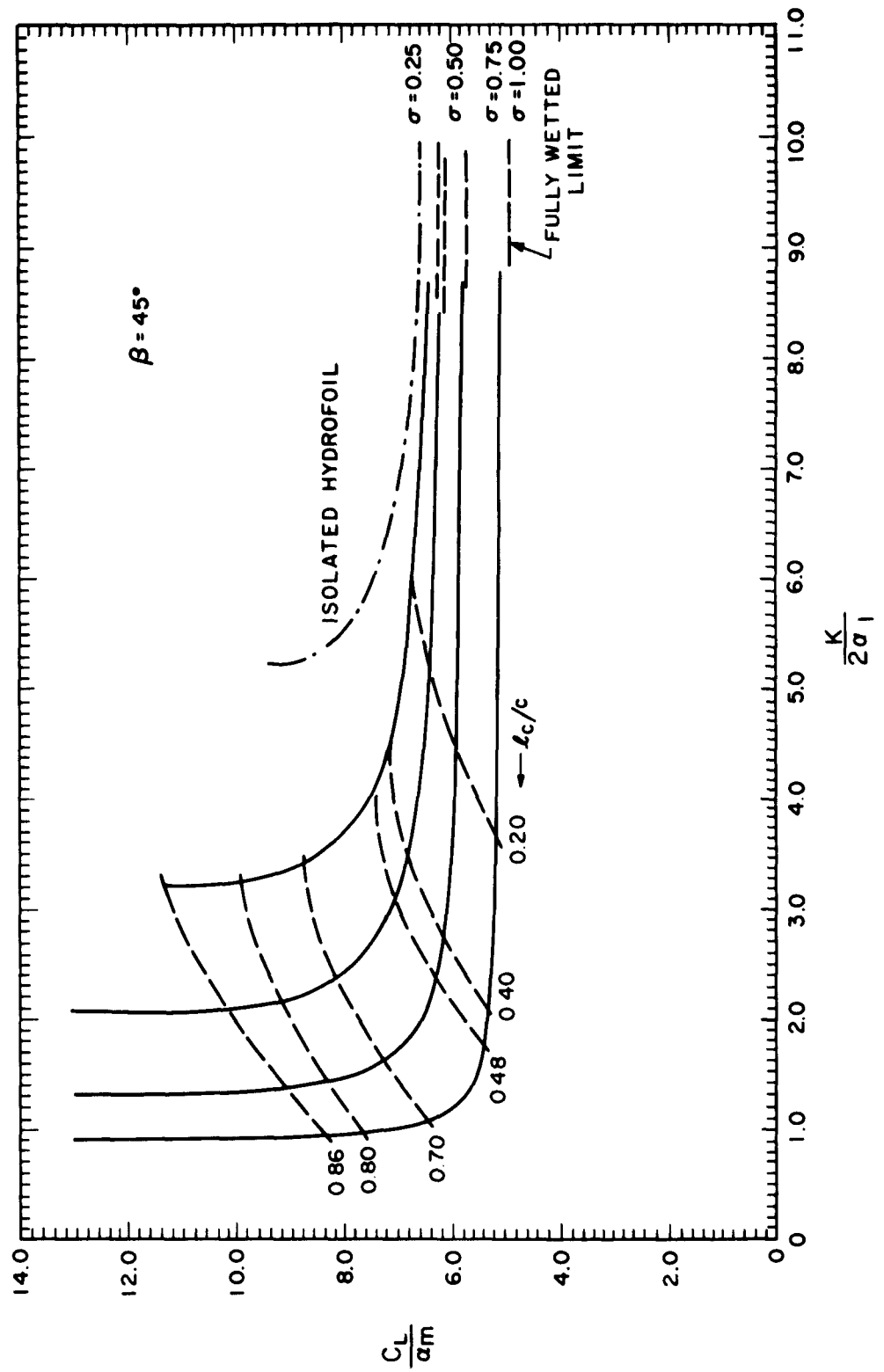


Fig. 20 Ratio of lift coefficient to mean flow angle vs. ratio of cavitation number to twice inlet angle for various solidities at a given stagger angle $\beta = 45^\circ$.

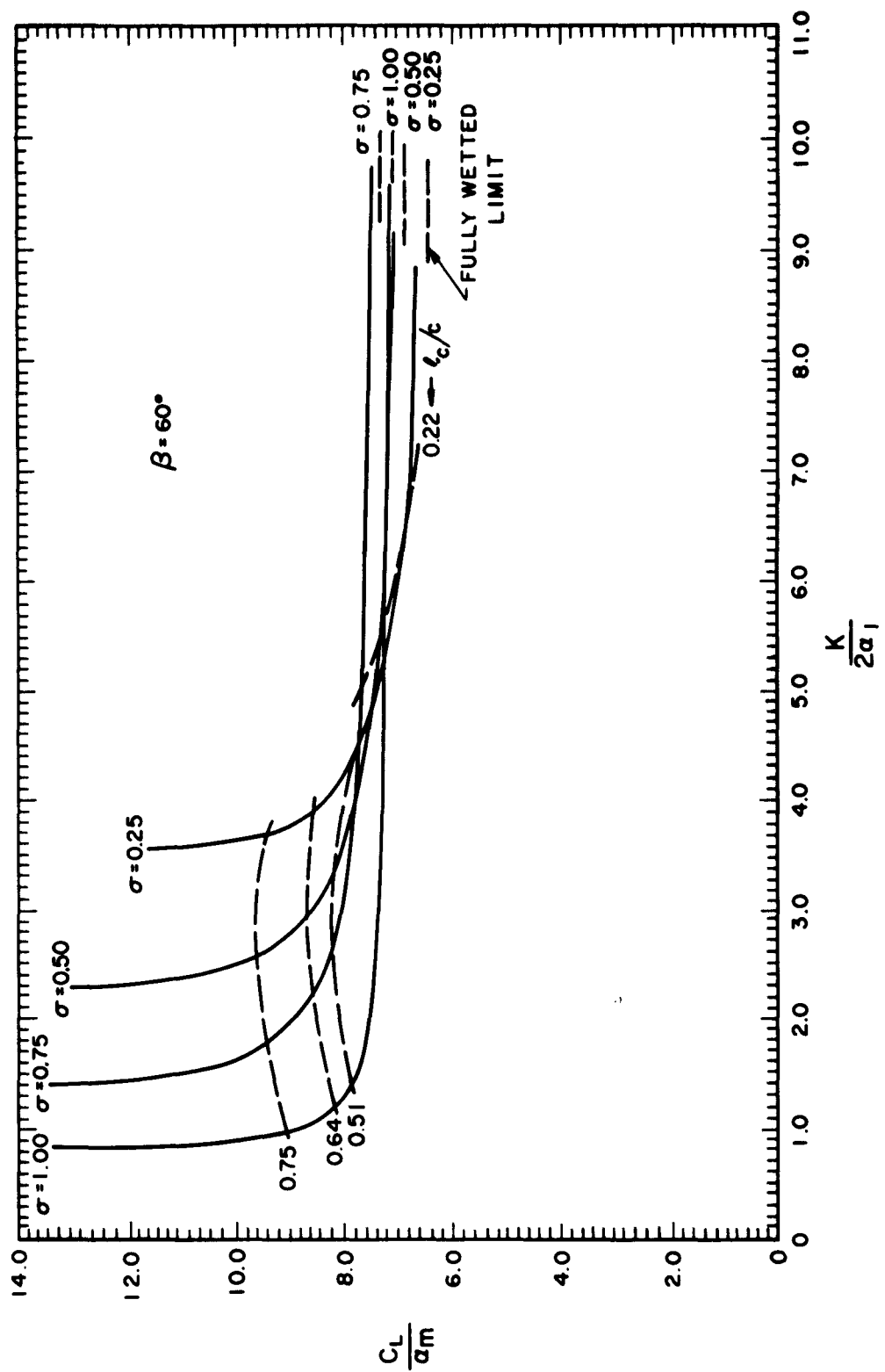


Fig. 21 Ratio of lift coefficient to mean flow angle vs. ratio of cavitation number to twice inlet angle for various solidities at a given stagger angle $\beta = 60^\circ$.

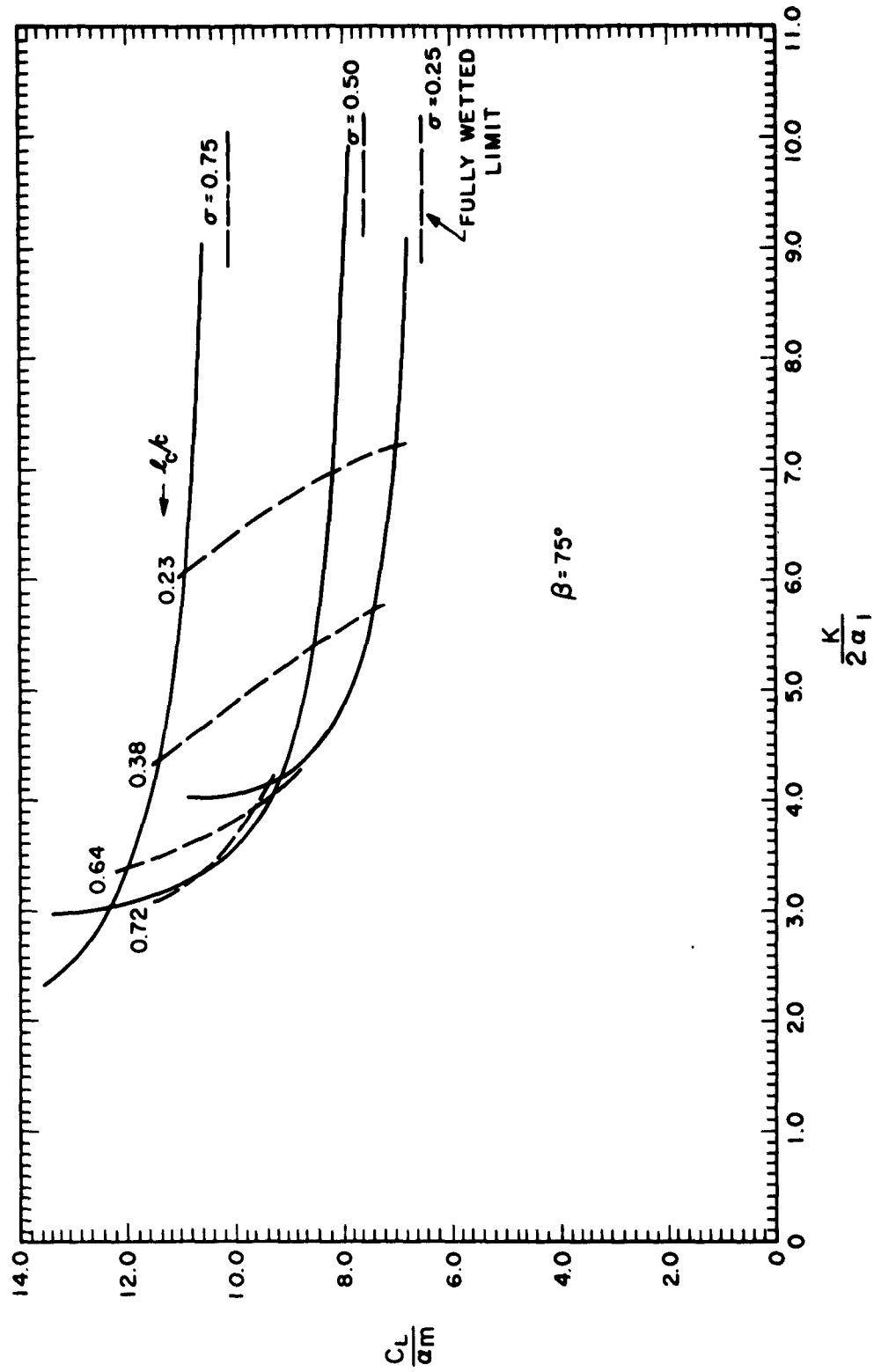


Fig. 22 Ratio of lift coefficient to mean flow angle vs. ratio of cavitation number to twice inlet angle for various solidities at a given stagger angle $\beta = 75^\circ$.

SOLIDITY $\sigma = 0.25$

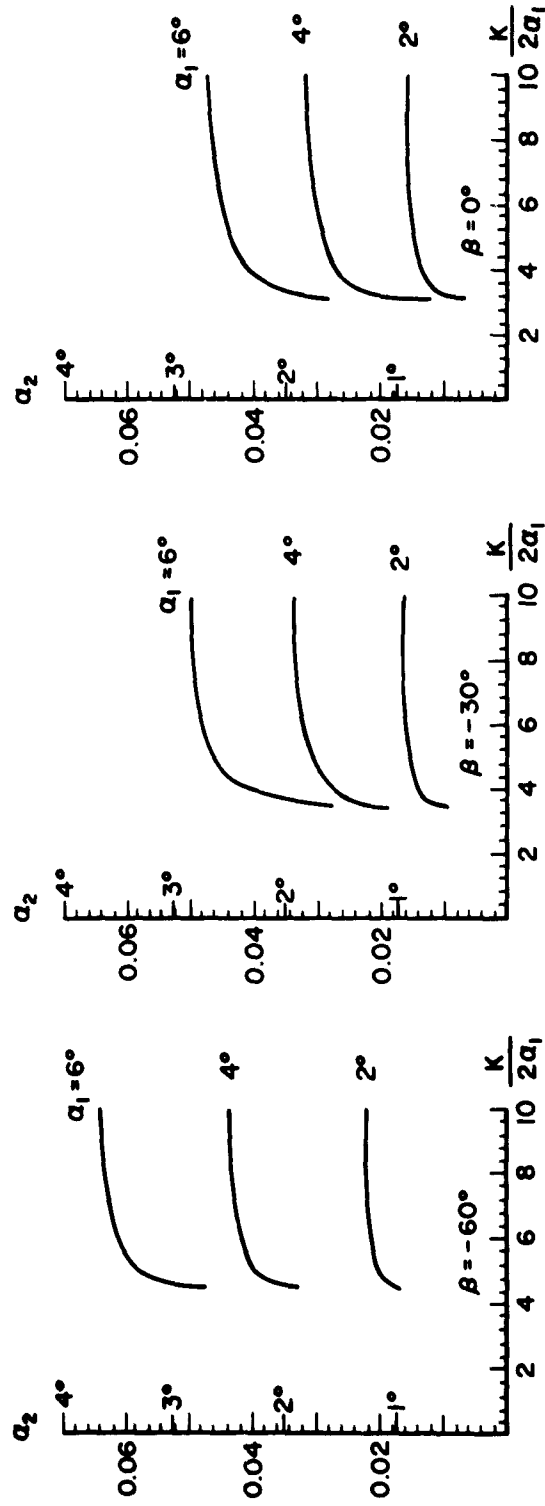


Fig. 23 Outlet flow angle vs. ratio of cavitation number to twice inlet angle for different inlet angles, at constant stagger angle.

SOLIDITY $\sigma = 0.25$

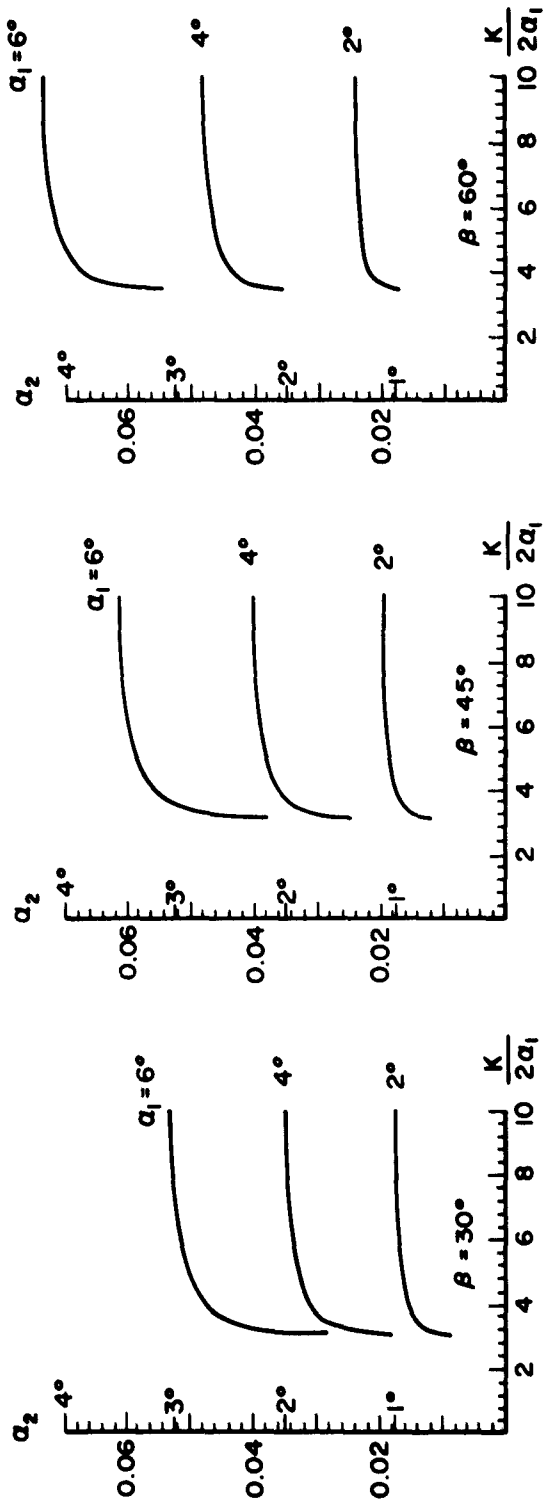


Fig. 23 Outlet flow angle vs. ratio of cavitation number to twice inlet angle for different inlet angles, at constant stagger angle.

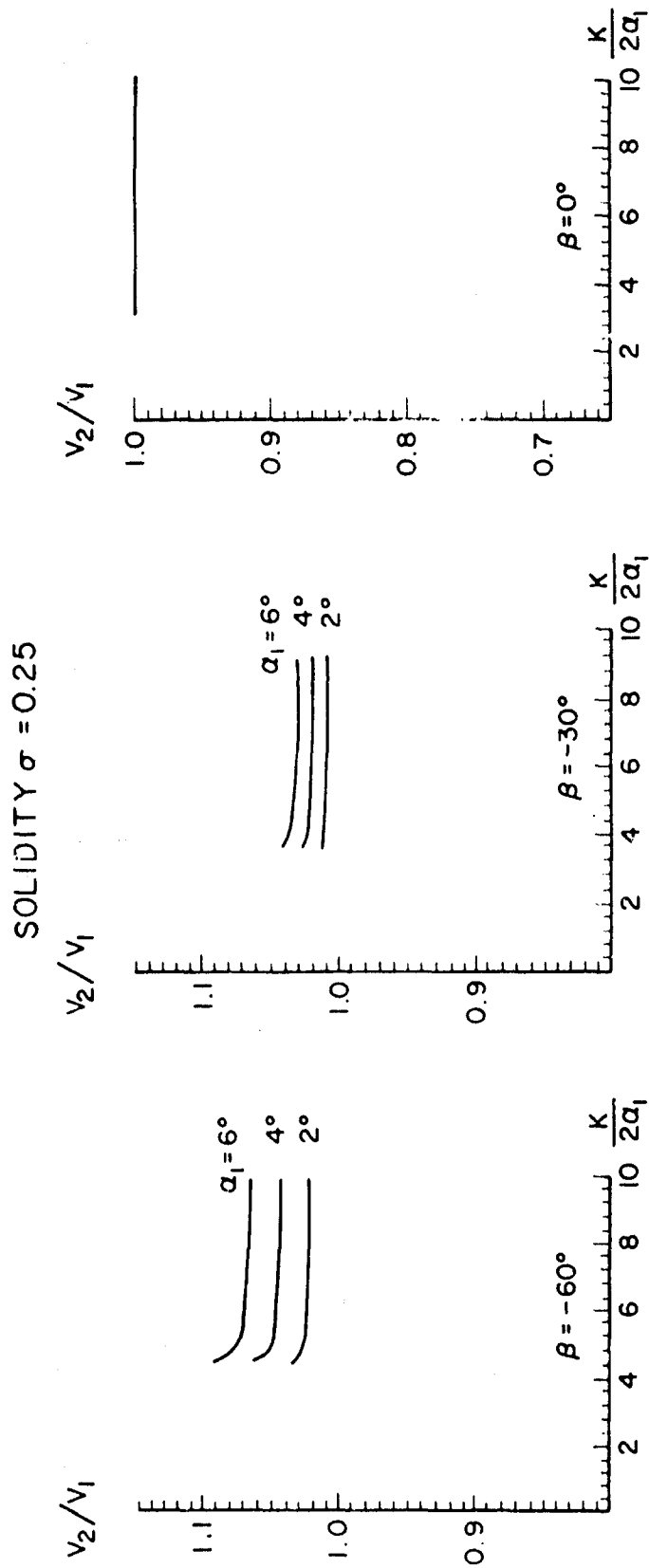


Fig. 24 Ratio of downstream velocity to upstream velocity vs. ratio of cavitation number to twice inlet angle for different inlet angles, at constant stagger angle.

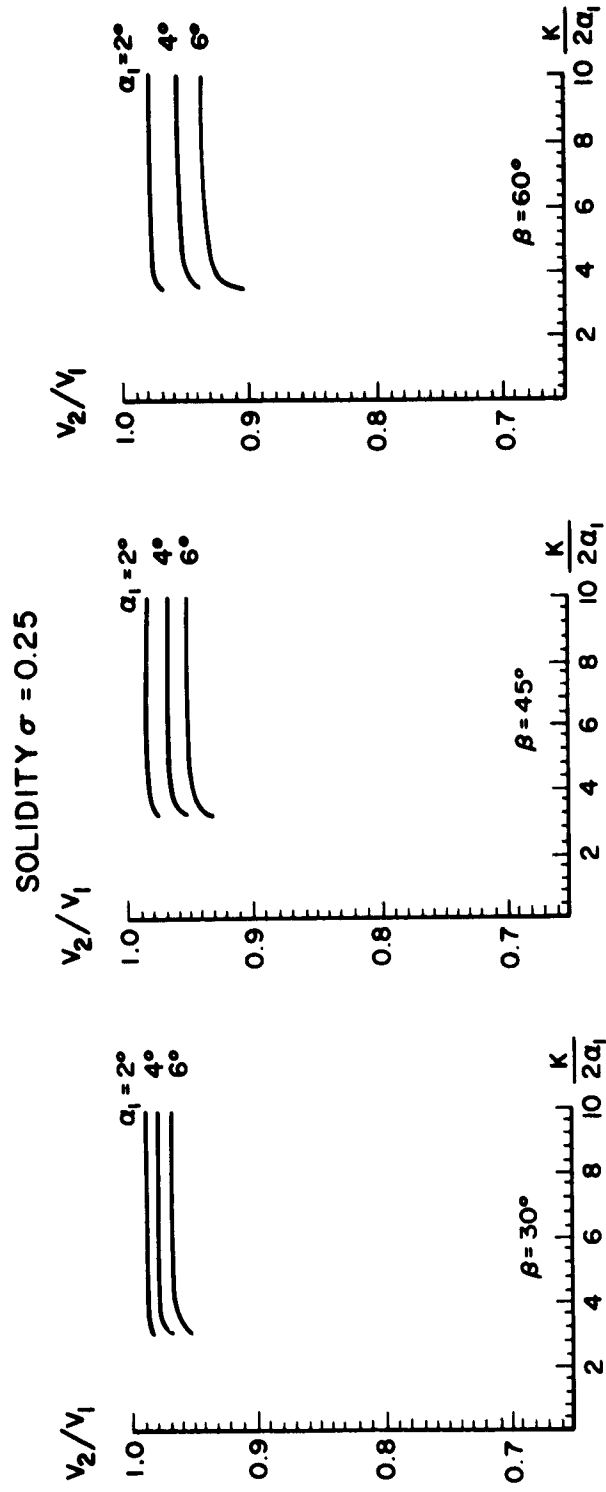


fig. 24 Ratio of downstream velocity to upstream velocity vs. ratio of cavitation number to twice inlet angle for different inlet angles, at constant stagger angle.

SOLIDITY $\sigma = 0.50$

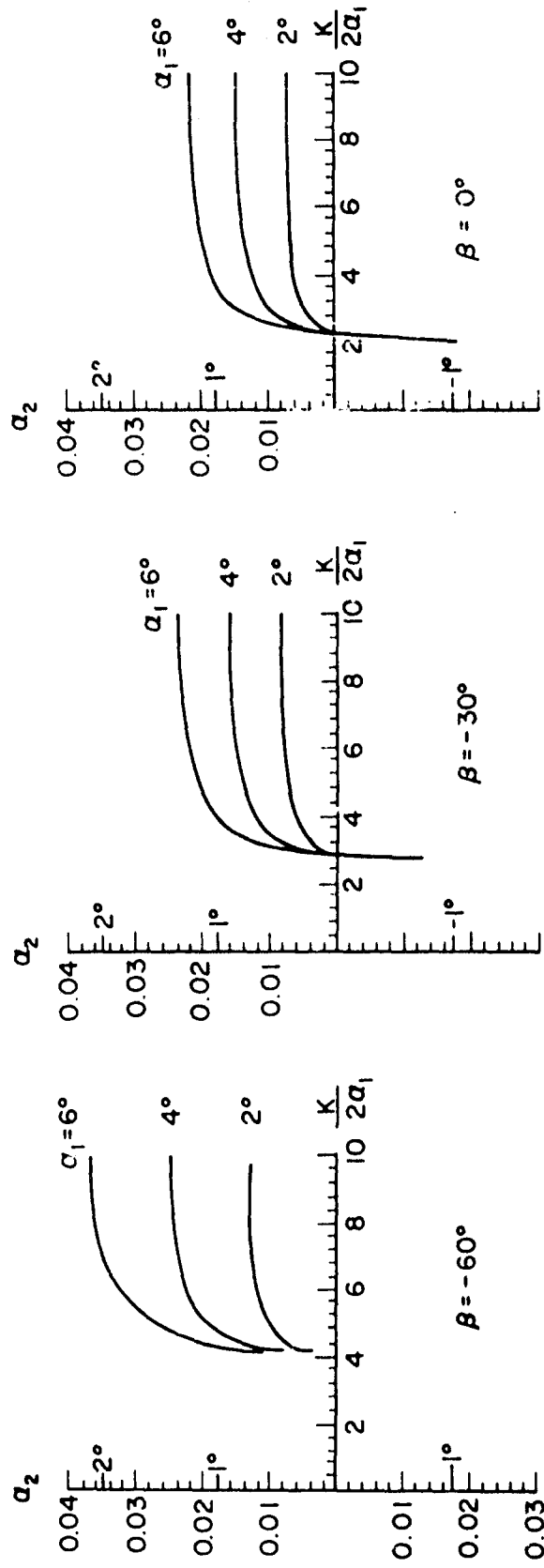


Fig. 25 Outlet flow angle vs. ratio of cavitation number to twice inlet angle for different inlet angles, at constant stagger angle.

SOLIDITY $\sigma = 0.50$

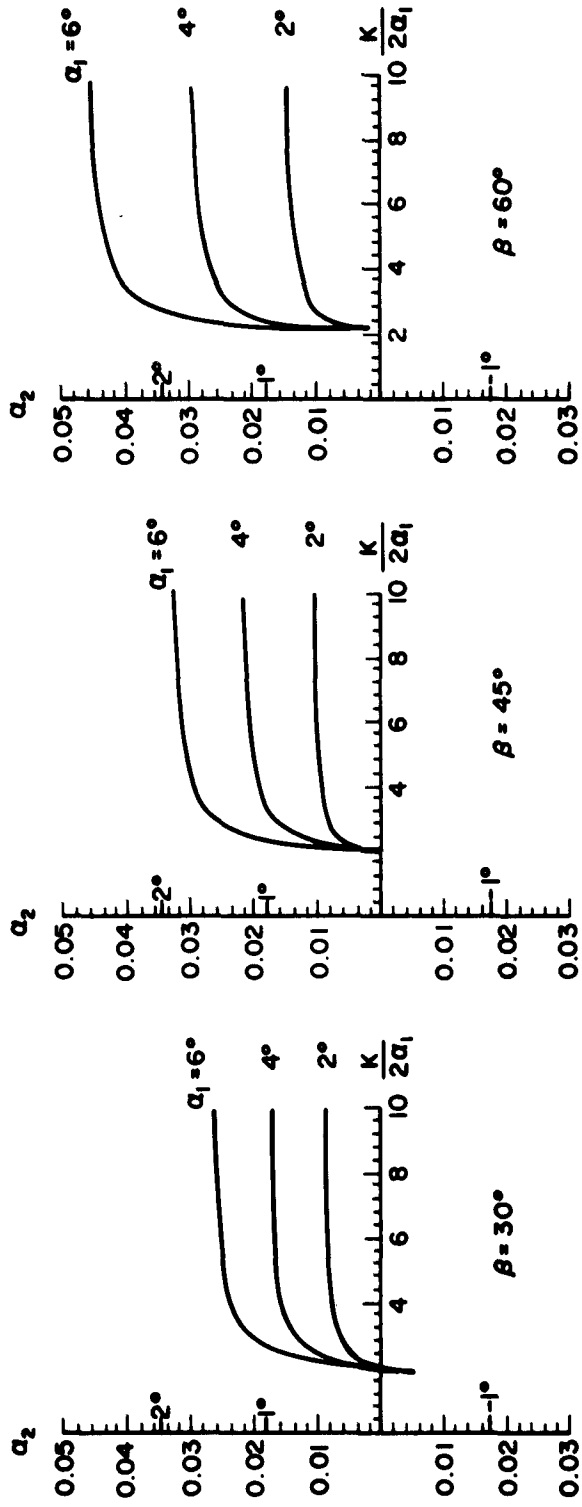


Fig. 25 Outlet flow angle vs. ratio of cavitation number to twice inlet angle for different inlet angles, at constant stagger angle.

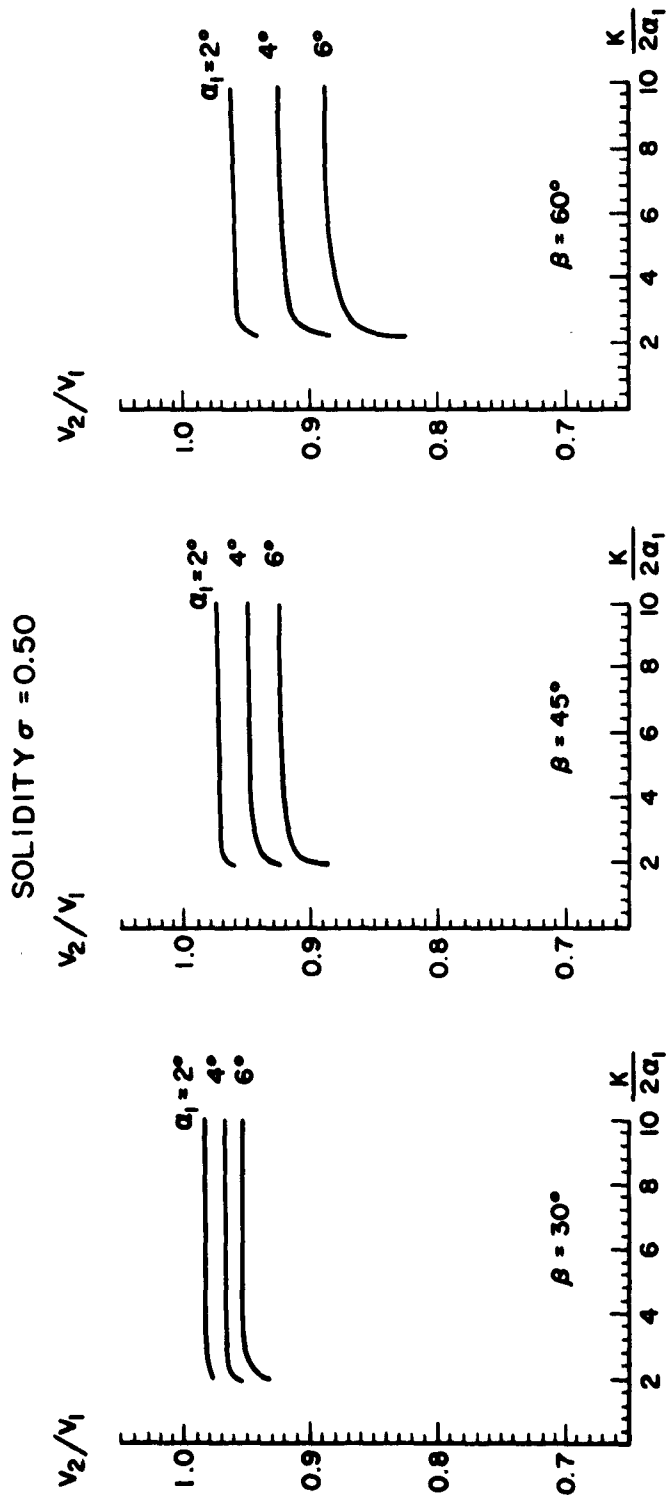


Fig. 26 Ratio of downstream velocity to upstream velocity vs. ratio of cavitation number to twice inlet angle for different inlet angles, at constant stagger angle.

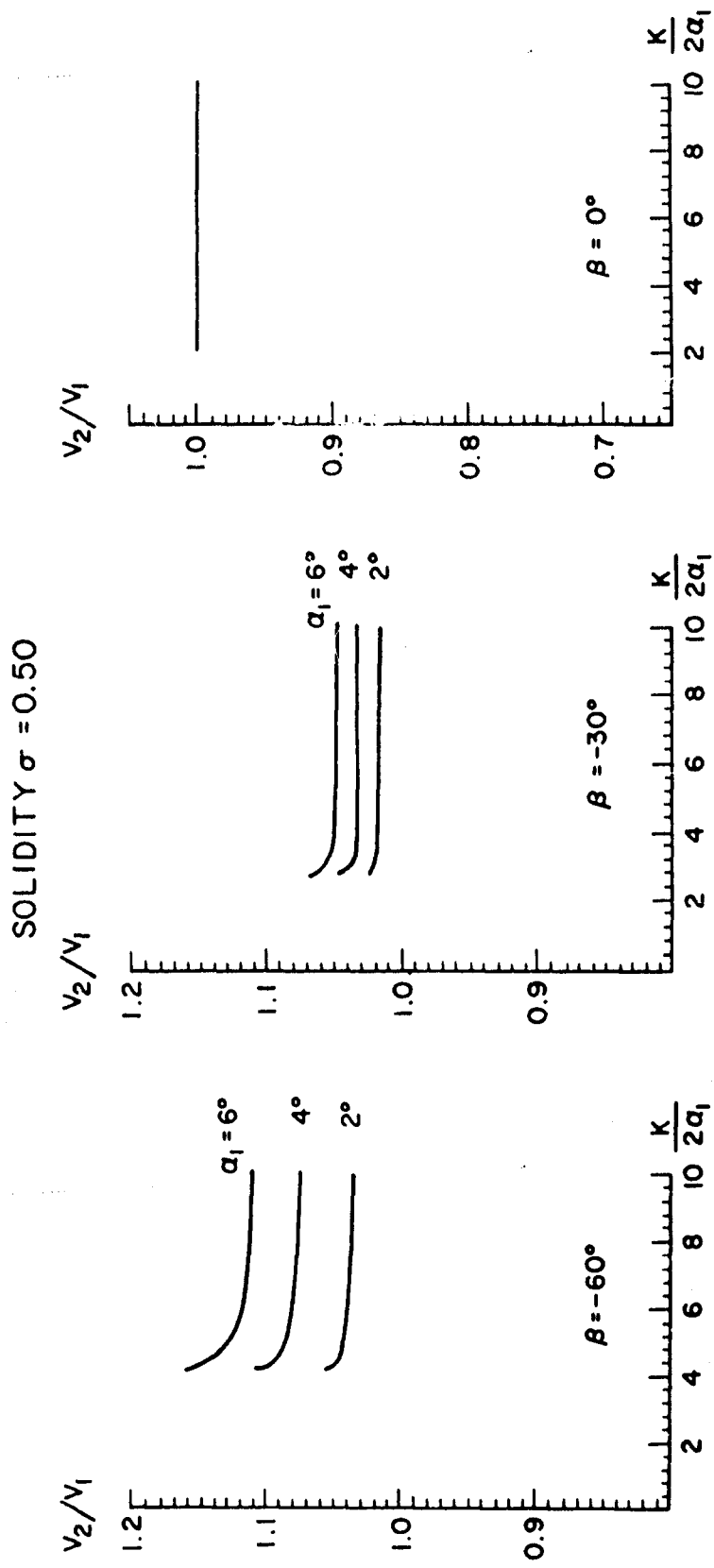


Fig. 26 Ratio of downstream velocity to upstream velocity vs. ratio of cavitation number to twice inlet angle for different inlet angles, at constant stagger angle.

SOLIDITY $\sigma = 0.75$

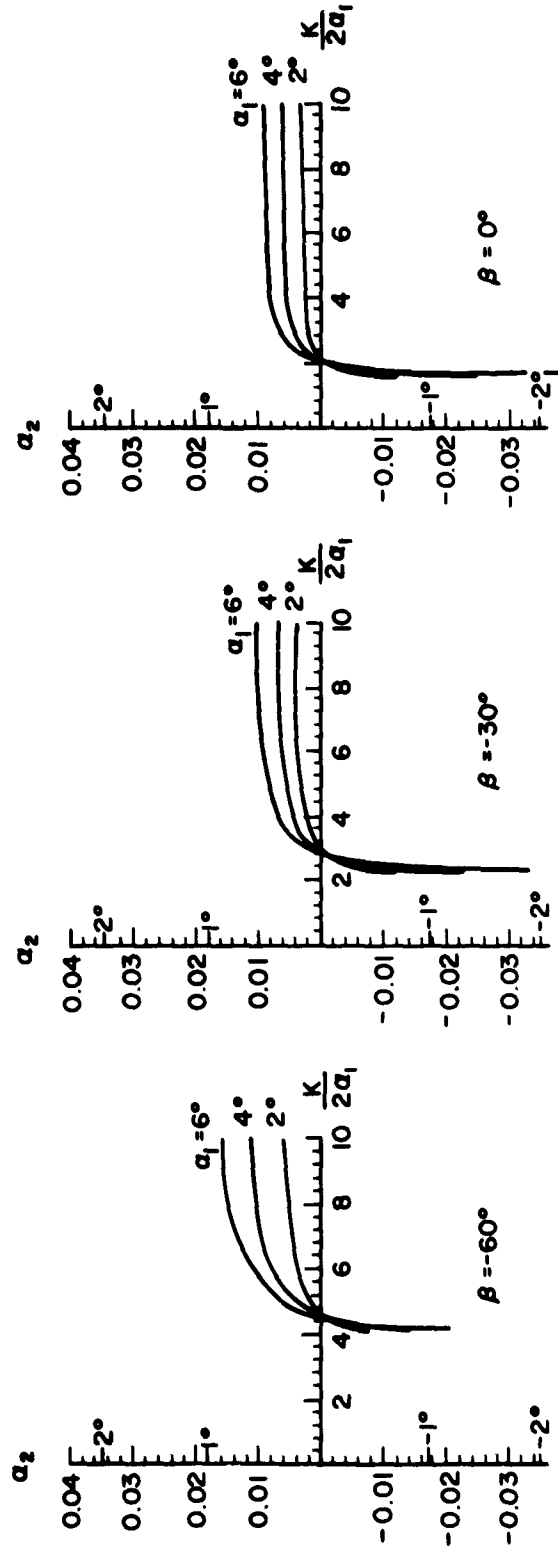


Fig. 27 Outlet flow angle vs. ratio of cavitation number to twice inlet angle for different inlet angles, at constant stagger angle.

SOLIDITY $\sigma = 0.75$

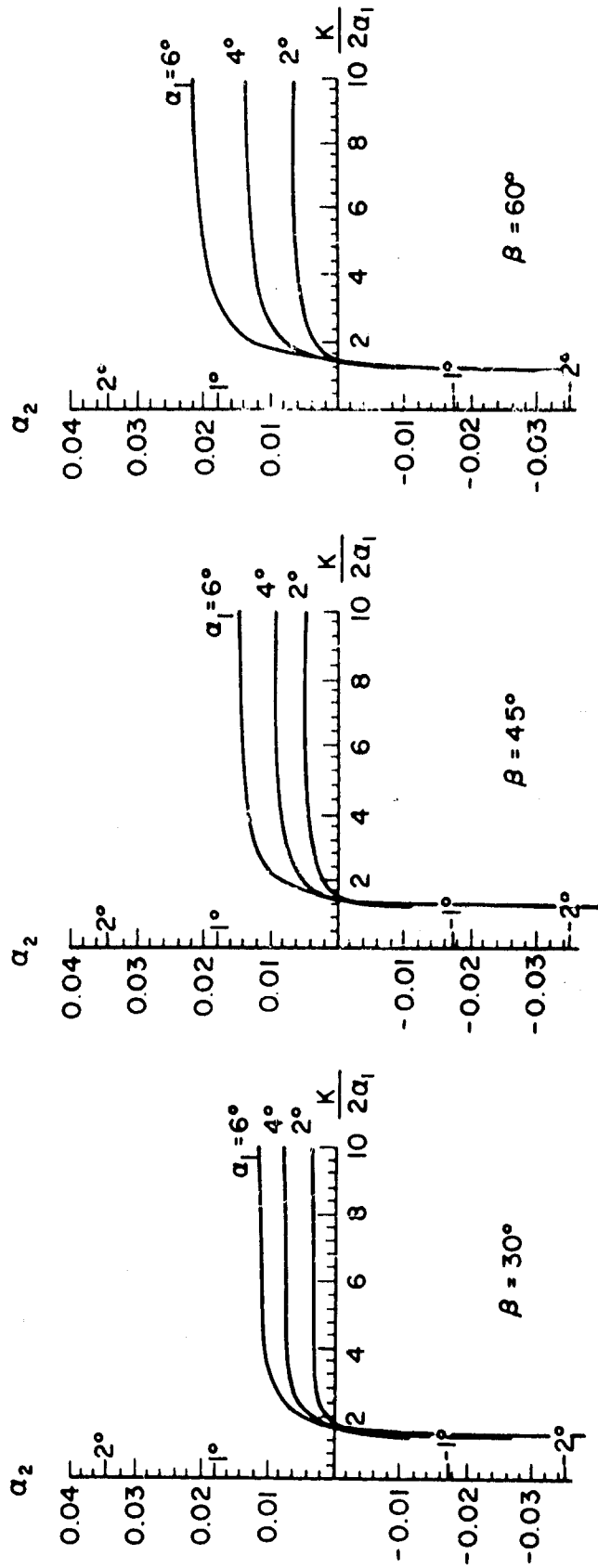


Fig. 27 Outlet flow angle vs. ratio of cavitation number to twice inlet angle for different inlet angles, at constant stagger angle.

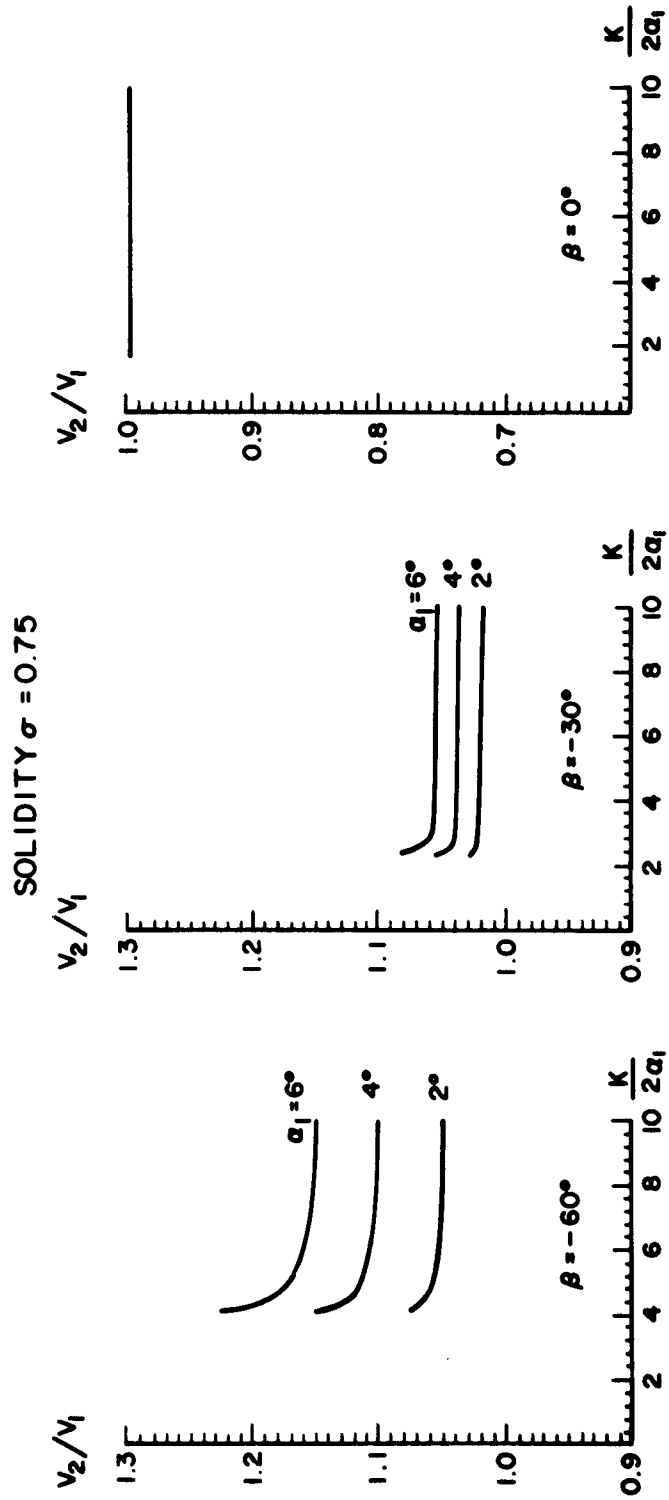


Fig. 28 Ratio of downstream velocity to upstream velocity vs. ratio of cavitation number to twice inlet angle for different inlet angles, at constant stagger angle.

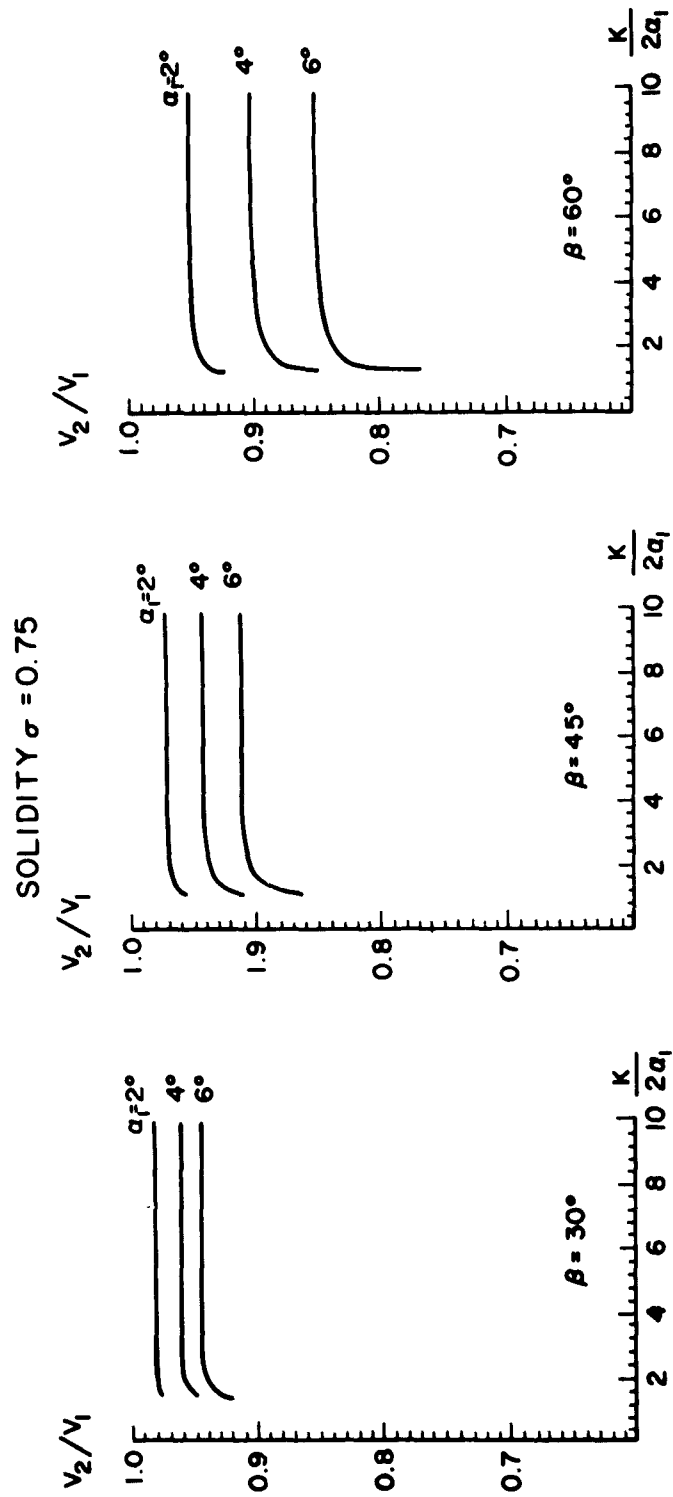


Fig. 28 Ratio of downstream velocity to upstream velocity vs. ratio of cavitation number to twice inlet angle for different inlet angles, at constant stagger angle.

**DISTRIBUTION LIST FOR UNCLASSIFIED REPORTS AND PREPRINTS ISSUED
UNDER CONTRACT Nonr (220(24) (NR 062-010)**

<p>Chief of Naval Research Department of the Navy Washington 25, D.C. Attn: Codes: 429 (1) 460 (1) 438 (3)</p>	<p>Chief, Bureau of Ships Department of the Navy Washington 25, D.C. Attn: Codes: 300 (R.A. A.M. Morgan) (1) 421 (Mr. J. Neidermair) (1) 440 (Mr. R.B. Couch) (1) 532 (1) 549 (1)</p>
<p>Commanding Officer Office of Naval Research Branch Office The John Crerar Library Building 86 East Randolph Street Chicago 1, Illinois (1)</p>	<p>Chief, Bureau of Yards and Docks Department of the Navy Washington 25, D.C. Attn: Comdr. A.S. Klay, Research Div.(1)</p>
<p>Commanding Officer Office of Naval Research Branch Office 346 Broadway New York 13, New York (1)</p>	<p>Commanding Officer and Director David Taylor Model Basin Washington 7, D.C. (1)</p>
<p>Commanding Officer Office of Naval Research Branch Office 1030 East Green Street Pasadena, California (1)</p>	<p>Commander Naval Ordnance Laboratory White Oak, Maryland (1)</p>
<p>Commanding Officer Office of Naval Research Navy No. 100, Fleet Post Office New York, New York (25)</p>	<p>Commander Naval Ordnance Test Station 3202 E. Foothill Blvd. Pasadena, California Attn: Head, Underwater Ordnance Dept.(1) Head, Propulsion Division (1)</p>
<p>Director Naval Research Laboratory Washington 25, D.C. Attn: Code 2021 (6)</p>	<p>Commanding Officer Naval Underwater Ordnance Station Newport, Rhode Island (1)</p>
<p>Chief, Bureau of Aeronautics Department of the Navy Washington 25, D.C. Attn: Code RS-3 (Mr. F.W.S. Locke)(1)</p>	<p>Commanding Officer and Director U.S. Naval Engineering Experiment Station Annapolis, Maryland (1)</p>
<p>Chief, Bureau of Ordnance Department of the Navy Washington 25, D.C. Attn: Codes: Re03 (Mr. J.D. Nicolaides) (1) ReU1 (Mr. C.S. Sandler) (1)</p>	<p>Superintendent U.S. Naval Postgraduate School Monterey, California (1)</p>
	<p>Commanding Officer and Director U.S. Naval Civil Engineering Laboratory Port Hueneme, California Attn: Code L54 (1)</p>
	<p>Director of Research NASA 1512 H Street, N.W. Washington 25, D.C. (1)</p>

Director Langley Aeronautical Laboratory NASA Langley Field, Virginia Attn: Mr. J.B. Parkinson, Hydrodynamics Division (1)	Mr. C.G. Morse, Chairman Maritime Administration 441 G Street, N.W. Washington, D.C. (1)
Director Lewis Flight Propulsion Laboratory NASA 21000 Brookpark Road Cleveland 11, Ohio (1)	ASTIA Document Service Center Arlington Hall Station Arlington 12, Virginia (5)
Commander Air Force Office of Scientific Res. Tempo T, 14th and Constitution Washington 25, D.C. Attn: Mechanics Division (1)	Office of Technical Services Department of Commerce Washington, D.C. (1)
Director Waterways Experiment Station Box 631 Vicksburg, Mississippi (1)	Polytechnic Institute of Brooklyn Department of Aeronautical Engineering and Applied Mechanics 99 Livingston Street Brooklyn 2, New York Attn: Professor A. Ferri (1)
Beach Erosion Board U.S. Army Corps of Engineers 5200 Little Falls Road Washington 26, D.C. (1)	Brown University Providence, Rhode Island Attn: Division of Applied Mathematics Professor L.M. Milne-Thomson (1) Division of Engineering Professor D. Drucker (1)
Office of Ordnance Research Department of the Army Washington 25, D.C. (1)	California Institute of Technology Pasadena, California Attn: Dean F. Lindvall (1) GALCIT Professor C.B. Millikan (1) Professor D. Rannie (1) Professor M.S. Plesset (1)
Office of the Chief of Engineers Department of the Army Gravelly Point Washington 25, D.C. (1)	University of California Berkeley 4, California Attn: Department of Engineering Professor A. Schade (1) Professor H. Einstein (1)
Major General P.F. Yount Chief of Transportation Department of the Army Washington 25, D.C. (1)	Carnegie Institute of Technology Pittsburgh, Pennsylvania Attn: Dean B. Teare, Jr. (1) Department of Mathematics (1)
Commissioner Bureau of Reclamation Washington 25, D.C. (1)	Case Institute of Technology Cleveland, Ohio Attn: Department of Mech. Engineering Professor G. Kuerti (1)
Dr. J.H. McMillen, Director National Science Foundation 1520 H. Street, N.W. Washington, D.C. (5)	Colorado A and M Fort Collins, Colorado Attn: Department of Civil Engineering Professor M. Albertson (1)
Director National Bureau of Standards Washington 25, D.C. Attn: Fluid Mechanics Division Dr. G.B. Schubauer (1) Dr. G.H. Keulegan (1)	

Columbia University
Dept. of Civil Engineering and
Engineering Mechanics
New York, New York
Attn: Professor R. Skalak (1)

Cornell University
Ithaca, New York
Attn: Graduate School of
Aeronautical Engineering
Professor W. Sears, Dir. (1)

Harvard University
Cambridge 38, Massachusetts
Attn: Department of Engineering
Sciences
Professor G. Carrier (1)

University of Illinois
Urbana, Illinois
Attn: College of Engineering
Professor J. Robertson (1)

Iowa Institute of Hydraulic Res.
State University of Iowa
Iowa City, Iowa
Attn: Dr. H. Rouse, Director (1)

Johns Hopkins University
Baltimore 18, Maryland
Attn: Department of Mechanical
Engineering
Professor S. Corrsin, Head (1)

University of Maryland
College Park, Maryland
Attn: Institute for Fluid Mechanics
Professor J. Weske (1)

Massachusetts Institute of Technology
Cambridge 39, Massachusetts
Attn: Department of Naval Architecture
and Marine Engineering
Professor L. Troost (1)
Professor M. Abkowitz (1)
Department of Civil Engineering
Professor A. Ippen (1)
Department of Mech. Engineering
Professor E.S. Taylor (1)

University of Michigan
Ann Arbor, Michigan
Attn: Applied Mechanics Department
Professor R. Dodge (1)

University of Minnesota
Minneapolis 14, Minnesota
Attn: St. Anthony Falls Hydraulic Lab.
Professor L. Straub, Dir. (1)

University of Notre Dame
Notre Dame, Indiana
Attn: College of Engineering
Dean K. Schoenherr (1)

Pennsylvania State University
University Park, Pennsylvania
Attn: Ordnance Research Laboratory
Professor G. Wislicenus (1)

Rensselaer Polytechnic Institute
Troy, New York
Attn: Department of Mathematics
Professor R. C. DiPrima (1)

Rose Polytechnic Institute
R.R. No. 5
Terre Haute, Indiana
Attn: Dr. W.W. Clauson (1)

University of Southern California
Department of Mechanical Engineering
Los Angeles 7, California
Attn: Professor R. C. Binder (1)

Stanford University
Stanford, California
Attn: Department of Civil Engineering
Professor J. Vennard (1)
Department of Mathematics
Professor M. Schiffer, Head (1)
Professor D. Gilbarg (1)

Stevens Institute of Technology
711 Hudson Street
Hoboken, New Jersey
Attn: Dr. J. Breslin (1)

University of Tennessee
Knoxville, Tennessee
Attn: Engineering Experimental
Station
Dr. G. Hickox, Director (1)

Western Res. University
Millis Science Center
Cleveland 6, Ohio
Attn: Professor W. Leighton, Jr. (1)

Worcester Polytechnic Institute Worcester, Massachusetts Attn: Alden Hydraulic Laboratory Professor J. Hooper, Dir. (1)	Republic Aviation Corporation Farmingdale, Long Island, N. Y. (1)
Aerojet General Corporation 6352 North Irwindale Avenue Azusa, California Attn: Mr. J. Levy (1)	EDO Corporation College Point, New York Attn: Mr. S. Fenn (1)
General Dynamics Corporation Convair Division 3165 Pacific Highway San Diego 12, California Attn: Mr. H. Brooks (1)	General Electric Company Pittsfield, Massachusetts Attn: Mr. R.H. Wahlberger (1)
The Glenn L. Martin Company Baltimore 3, Maryland Attn: Mr. J. Pearson (1)	Philco Corporation 4700 Wissahickon Avenue Philadelphia, Pennsylvania Attn: Mr. M. Arsove (1)
North American Aviation, Inc. International Airport Los Angeles 45, California (1)	Vitro Corporation of America 962 Wayne Avenue Silver Spring, Maryland Attn: Mr. V. Setterholm (1)
Lockheed Aircraft Corporation 2555 N. Hollywood Way Burbank, California (1)	Westinghouse Electric Corporation Sharon, Pennsylvania Attn: Mr. M.E. Fagan (1)
Boeing Airplane Company Scientific Research Laboratories P.O. Box 3981 Seattle 24, Washington (1)	AVCO Manufacturing Corporation Stamford, Connecticut (1)
Hughes Aircraft Company Florence and Teale Culver City, California (1)	Gibbs and Cox 21 West Street New York 6, New York Attn: Dr. S. Hoerner (1)
Douglas Aircraft Company, Inc. El Segundo, California (1)	Bethlehem Steel Company Shipbuilding Division Quincy 69, Massachusetts Attn: Mr. H. deLuce (1)
Bell Aircraft Corporation P.O. Box No. 1 Buffalo 5, New York (1)	General Dynamics Corporation Electric Boat Division Groton, Connecticut Attn: R.A. A.I. McKee, USN (ret.) (1)
McDonnell Aircraft Corporation P.O. Box No. 516 St. Louis 3, Missouri (1)	International Business Machines Corp. 112 East Post Road White Plains, New York Attn: Dr. H. Cohen (1)
Chance Vought Aircraft, Inc. P.O. Box No. 5907 Dallas, Texas (1)	Dynamic Developments Corporation St. Marks Lane Islip, Long Island, New York Attn: Mr. W. Carl (1)
Northrop Aircraft, Inc. Northrop Field Hawthorne, California (1)	Miami Shipbuilding Corporation 615 S.W. Second Avenue Miami 36, Florida Attn: Mr. P. Buhler (1)
Grumman Aircraft Eng. Corp. Bethpage, Long Island, N. Y. (1)	

Baker Manufacturing Company Evansville, Wisconsin Attn: Mr. J. Baker	(1)	Hydronautics, Incorporated Pindell School Road Howard County Laurel, Maryland Attn: Mr. Phillip Eisenberg Mr. Marshall P. Tulin	(1) (1)
Eastern Research Group 215 Montague Street Brooklyn 1, New York Attn: Dr. L. Meyerhoff	(1)	Oceanics, Incorporated 114 East 40th Street New York 16, N.Y. Attn: Mr. Paul Kaplan, President	(1) (1)
Aircraft Gas Turbine Division General Electric Company Cincinnati 15, Ohio Attn: Dr. M.L. Ghai	(1)	Morris Machine Works Baldwinsville, New York Attn: Mr. Fred F. Antunes Hydraulic Engineer	(1) (1)
Aircraft Gas Turbine Development Dept. Malta Test Station Ballston Spa, New York Attn: Mr. Kurt Berman	(1)	Monsanto Chemical Company 800 N. Lindberg Blvd. St. Louis 66, Missouri Attn: Mr. R. Dean	(1) (1)
Rocketdyne 6633 Canoga Avenue Canoga Park, California Attn: Librarian, Dept. 596-3	(1)	Professor H.G. Flynn Department of Electrical Engineering University of Rochester College of Engineering River Campus Station Rochester 20, New York	(1) (1)
Technical Research Group, Inc. 2, Aerial Way Syosset, New York Attn: Dr. J. Kotik	(1)		